


Spring 2017

# Synthesis, Kinetic and Catalytic Studies of Manganese Complexes with Corrole and Porphyrin Ligands

Haleh Jeddi

Western Kentucky University, haleh.jeddi231@topper.wku.edu

Follow this and additional works at: <http://digitalcommons.wku.edu/theses>

 Part of the [Biochemistry Commons](#), and the [Inorganic Chemistry Commons](#)

---

## Recommended Citation

Jeddi, Haleh, "Synthesis, Kinetic and Catalytic Studies of Manganese Complexes with Corrole and Porphyrin Ligands" (2017). *Masters Theses & Specialist Projects*. Paper 1949.

<http://digitalcommons.wku.edu/theses/1949>

This Thesis is brought to you for free and open access by TopSCHOLAR®. It has been accepted for inclusion in Masters Theses & Specialist Projects by an authorized administrator of TopSCHOLAR®. For more information, please contact [topscholar@wku.edu](mailto:topscholar@wku.edu).

SYNTHESIS, KINETIC AND CATALYTIC STUDIES OF MANGANESE  
COMPLEXES WITH CORROLE AND PORPHYRIN LIGANDS

A Thesis  
Presented to  
The Faculty of the Department of Chemistry  
Western Kentucky University  
Bowling Green, Kentucky

In Partial Fulfillment  
Of the Requirements for the Degree  
Master of Science

By  
Haleh Jeddi

May 2017


SYNTHESIS, KINETIC AND CATALYTIC STUDIES OF MANGANESE  
COMPLEXES WITH CORROLE AND PORPHYRIN LIGANDS

Date Recommended 4-11-17

  
\_\_\_\_\_  
Dr. Rui Zhang, Director of Thesis

  
\_\_\_\_\_  
Dr. Kevin Williams

  
\_\_\_\_\_  
Dr. Matthew Nee

  
\_\_\_\_\_  
Dean, Graduate School

4/18/17  
Date

## ACKNOWLEDGEMENTS

I would first like to acknowledge my adviser, Dr. Rui Zhang, for his support. His patience, encouragement and advice were invaluable to me, both in academics and in my personal life. I could not have asked for a better research adviser. I would also like to acknowledge my colleagues and friends in my research group.

I am grateful for the help of my committee members, Dr. Kevin Williams and Dr. Matthew Nee. Dr. Nee has been especially helpful as an academic adviser. I would also like to acknowledge Dr. Stuart Burris for his help with cyclic voltammetry and Dr. Lester Pesterfield for support with the NMR. I am also grateful for the help of Ms. Alicia Pesterfield, both in the stockroom and in teaching. I sincerely appreciate the help of Ms. Haley Smith, whose advice and moral support have been invaluable.

This thesis would not have been possible without my family and my closest friends, Aubrey and Sara. Their emotional support during the writing of this thesis, as well as in frantic study sessions and graduate school applications, made this process much easier.

This work was funded by the NSF (CHE 1464886) and a WKU internal grant (FUSE 15-FA257). I would like to acknowledge the WKU Department of Chemistry for support in the form of a Teaching Assistantship.

## CONTENTS

LIST OF FIGURES .....	vi
LIST OF TABLES .....	viii
LIST OF SCHEMES .....	ix
ABSTRACT .....	x
1. INTRODUCTION.....	1
1.1 Cytochrome P450 Enzymes.....	1
1.2 High-Valent Transition Metal-Oxo Species in Catalytic Oxidations .....	5
1.3 Metalloporphyrins as Biomimetic Catalysts.....	6
1.4 Manganese Corroles as Biomimetic Catalysts .....	7
1.5 Significance of Sulfoxidation Reactions .....	9
2. EXPERIMENTAL SECTION .....	11
2.1 Materials .....	11
2.2 General Procedures.....	11
2.2.1 Physical Measurements.....	11
2.2.2 Catalytic Oxidations.....	12
2.3 Synthesis and Spectroscopic Characterization .....	12
2.3.1 Tris(pentafluorophenyl)corrole (H <sub>3</sub> TPFC, <b>1a</b> ) .....	12
2.3.2 Triphenylcorrole (H <sub>3</sub> TPC, <b>1b</b> ) .....	15
2.3.3 <i>meso</i> -Tetramesitylporphyrin (H <sub>2</sub> TMP, <b>1c</b> ) .....	17
2.3.4 Manganese(III) Corroles [Mn <sup>III</sup> (Cor)·(OEt <sub>2</sub> ) <sub>2</sub> , <b>2</b> ] .....	20

2.3.5 Manganese(III) Porphyrin Chloride [Mn <sup>III</sup> (TMP)Cl, <b>2c</b> ]	23
3. KINETIC STUDIES OF STOICHIOMETRIC OXIDATIONS BY Mn <sup>V</sup> (TPFC)O AND Mn <sup>IV</sup> (TMP)O	25
3.1 Introduction	25
3.2. Results and Discussion	25
3.2.1 Electrochemical Studies	25
3.2.2 Solvent Effect	28
3.2.3 Kinetic Studies of Oxidations by <b>3a</b>	33
3.2.4 Hammett Correlation Studies	38
3.3 Mechanistic Considerations	41
4. CATALYTIC OXIDATIONS BY MANGANESE CORROLES	44
4.1 Introduction	44
4.2 Screening Studies	45
4.2.1 Solvent Effect	45
4.2.2 Water Effect	49
4.3 Catalytic Oxidations of Sulfides to Sulfoxides	51
4.4 Catalytic Epoxidation of Alkenes	53
5. CONCLUSIONS	56
REFERENCES	58
CURRICULUM VITAE	66
LIST OF ABBREVIATIONS	67

## LIST OF FIGURES

Figure 1. The crystal structure of CYP450 <sub>cam</sub> . <sup>11</sup> .....	2
Figure 2. The structure of heme <i>b</i> , also called protoporphyrin IX. ....	4
Figure 3. General structure of metalloporphyrin catalysts. ....	7
Figure 4. The structures of the porphyrin, corrole and corrin ligands. ....	8
Figure 5. The <sup>1</sup> H-NMR spectrum of H <sub>3</sub> TPFC ( <b>1a</b> ) in CDCl <sub>3</sub> . ....	14
Figure 6. The UV-visible absorption spectrum of H <sub>3</sub> TPFC ( <b>1a</b> ) in CH <sub>2</sub> Cl <sub>2</sub> . ....	15
Figure 7. The <sup>1</sup> H-NMR spectrum of H <sub>3</sub> TPC ( <b>1b</b> ). ....	16
Figure 8. The UV-visible absorption spectrum of H <sub>3</sub> TPC ( <b>1b</b> ). ....	17
Figure 9. The <sup>1</sup> H-NMR spectrum of H <sub>2</sub> TMP ( <b>1c</b> ). ....	19
Figure 10. The UV-visible absorption spectrum of H <sub>2</sub> TMP ( <b>1c</b> ). ....	19
Figure 11. The <sup>1</sup> H-NMR spectrum of <b>2a</b> in CDCl <sub>3</sub> . ....	21
Figure 12. The UV-visible absorption spectrum of <b>2a</b> in CH <sub>2</sub> Cl <sub>2</sub> . ....	21
Figure 13. The <sup>1</sup> H-NMR spectrum of <b>2b</b> in CDCl <sub>3</sub> . ....	22
Figure 14. The UV-visible absorption spectrum of <b>2b</b> in CH <sub>2</sub> Cl <sub>2</sub> . ....	22
Figure 15. The <sup>1</sup> H-NMR spectrum of <b>2c</b> in CDCl <sub>3</sub> . ....	24
Figure 16. The UV-visible absorption spectrum of <b>2c</b> in CH <sub>2</sub> Cl <sub>2</sub> . ....	24
Figure 17. A cyclic voltammogram of <b>2a</b> (1 mM) in a 0.1 M TBAP/CH <sub>3</sub> CN solution at scan rate 100 mV/s and with a three-electrode system: a glassy carbon working electrode, a platinum wire counter electrode and an Ag <sup>+</sup> /AgNO <sub>3</sub> reference electrode. The E <sub>1/2</sub> of the system under these conditions is 385 mV. ....	26
Figure 18. A cyclic voltammogram of <b>2b</b> (1 mM) in a 0.1 M TBAP/CH <sub>3</sub> CN solution at scan rate 100 mV/s with a three-electrode system: a glassy carbon working electrode, a	

platinum wire counter electrode and a $\text{Ag}^+/\text{AgNO}_3$ reference electrode. The $E_{1/2}$ of the system under these conditions is 186 mV. ....	27
Figure 19. A Cottrell plot of the peak current of the oxidation of <b>2a</b> at varied scan rates. This plot is linear for diffusion-controlled electrochemical systems, and $k_{\text{ox}}$ is a collection of constants specific to the system. ....	28
Figure 20. The UV-visible absorption spectra of <b>3a</b> (left, solid line) generated by oxidation of <b>2a</b> (left, dashed line) with <i>m</i> -CPBA in $\text{CH}_3\text{CN}$ and <b>4c</b> (right, solid line) generated by oxidation of <b>2c</b> (right, dashed line). ....	30
Figure 21. Time-resolved UV-vis spectra of the decay of <b>3a</b> into <b>2a</b> in $\text{CH}_3\text{CN}$ in the presence or absence of substrate over 3 h. ....	31
Figure 22. Time-resolved spectra of the decay of <b>3a</b> in the presence or absence of substrate into a suspected $\text{Mn}^{\text{IV}}(\text{TPFC})\text{X}$ over 5 h. ....	32
Figure 23. Time-resolved spectra of the decay of <b>4c</b> into <b>2c</b> in $\text{CH}_3\text{CN}$ in the presence or absence of substrate over 20 min. ....	32
Figure 24. Kinetic traces monitored at $\lambda_{\text{max}} = 349$ nm, showing the decay of <b>3a</b> ( $2.5 \times 10^{-5}$ M) into <b>2a</b> in $\text{CH}_2\text{Cl}_2$ with varied concentrations of thioanisole: 10 mM (black), 20 mM (blue), 30 mM (red) and 40 mM (green). ....	34
Figure 25. A plot of the observed rate constants versus the concentration of thioanisole in $\text{CH}_3\text{CN}$ . Error bars are reported as $1\sigma$ . ....	35
Figure 26. The Hammett plot for oxidations of <i>p</i> -substituted thioanisoles by <b>3a</b> in $\text{CH}_3\text{CN}$ . ....	40
Figure 27. The Hammett plot for epoxidations of <i>p</i> -substituted styrenes by <b>4c</b> in $\text{CH}_3\text{CN}$ . ....	41



## LIST OF TABLES

Table 1. Kinetics of oxidation reactions by <b>3a</b> <sup>a</sup> .....	36
Table 2. Rate constants of OAT to <i>p</i> -substituted styrenes by <b>4c</b> <sup>a</sup> .....	37
Table 3. Rate constants of OAT to <i>p</i> -substituted thioanisoles by <b>3a</b> <sup>a</sup> .....	39
Table 4. Solvent effect on the epoxidation of <i>cis</i> -cyclooctene by <b>2a</b> <sup>a</sup> .....	46
Table 5. Solvent effect on the epoxidation of <i>cis</i> -cyclooctene by <b>2b</b> <sup>a</sup> .....	48
Table 6. Water effect on the epoxidation of <i>cis</i> -cyclooctene by <b>2a</b> <sup>a</sup> .....	50
Table 7. Water effect on the epoxidation of <i>cis</i> -cyclooctene by <b>2b</b> <sup>a</sup> .....	51
Table 8. Catalytic sulfoxidation of <i>p</i> -substituted thioanisoles by <b>2a</b> <sup>a</sup> .....	52
Table 9. Catalytic epoxidation of <i>p</i> -substituted styrenes by <b>2a</b> <sup>a</sup> .....	53
Table 10. Catalytic epoxidation of <i>p</i> -substituted styrenes by <b>2c</b> <sup>a</sup> .....	55

## LIST OF SCHEMES

Scheme 1. The specific hydroxylation of camphor on C5, producing only the <i>exo</i> product.....	3
Scheme 2. The catalytic cycle of CYP450 enzyme-catalyzed hydroxylation.....	4
Scheme 3. Typical oxidations catalyzed by metalloporphyrins. ....	5
Scheme 4. The oxidation of sulfides to sulfoxides with isolated Mn <sup>V</sup> TPFC(O).....	9
Scheme 5. The two-step synthesis of H <sub>3</sub> TPFC ( <b>1a</b> ).....	14
Scheme 6. The synthesis of H <sub>3</sub> TPC ( <b>1b</b> ).....	16
Scheme 7. The synthesis of H <sub>2</sub> TMP ( <b>1c</b> ). ....	18
Scheme 8. Synthesis of manganese(III) corrole complexes.....	20
Scheme 9. The proposed two-pathway mechanism of oxidation by <b>3a</b> . Pathway I is the direct oxidation, while II is the disproportionation pathway.....	42
Scheme 10. Catalytic sulfoxidations and epoxidations by manganese(III) corroles. ....	45

SYNTHESIS, KINETIC AND CATALYTIC STUDIES OF MANGANESE  
COMPLEXES WITH CORROLE AND PORPHYRIN LIGANDS

Haleh Jeddi

May 2017

68 Pages

Directed by: Dr. Rui Zhang, Dr. Kevin Williams, and Dr. Matthew Nee

Department of Chemistry

Western Kentucky University

High-valent transition metal-oxo intermediates play a significant role in the catalytic cycle of the ubiquitous cytochrome P450 enzymes and in biomimetic catalytic systems. In this work, manganese(III) porphyrin and corrole systems (**2**) were synthesized and characterized by UV-vis absorbance and <sup>1</sup>H-NMR, matching literature-reported spectroscopic data. Manganese(V)-oxo corroles (**3**) and a manganese(IV)-oxo porphyrin (**4**) were successfully generated by chemical oxidation using *m*-chloroperoxybenzoic acid (*m*-CPBA), and their oxidation reactions with organic reductants were comparatively investigated. Results from single-turnover kinetic studies indicate that in the tris(pentafluorophenyl)corrole system (**3a**), the active oxidizing intermediate differs in different solvents. The active oxidizing intermediate in acetonitrile is likely the manganese(V)-oxo species **3a**. However, in dichloromethane, the active oxidant is suspected to be a putative manganese(VI)-oxo species generated by disproportionation of the manganese(V)-oxo species.

Tris(pentafluorophenyl)corrolato manganese(III) (**2a**) was shown to selectively catalyze sulfoxidation and epoxidation with iodobenzene diacetate [PhI(OAc)<sub>2</sub>] as a mild oxygen source. **2a** exhibited higher conversions than triphenylcorrolato manganese(III) (**2b**), most likely because of the higher stability of **2a** compared to **2b**. In

contrast, tetramesitylporphyrinato manganese(III) (**2c**) was more efficient in catalytic oxidations than **2a**, resulting in much higher conversions, but much less selectivity. Other reported metalloporphyrin and metallocorrole systems show an accelerating effect upon addition of small amounts of water; however, neither corrole systems exhibited a positive water effect. This is attributed to the strong coordination between the manganese center and water, preventing the oxygen source from coordination.

# 1. INTRODUCTION

## 1.1 Cytochrome P450 Enzymes

The oxidation of organic substrates is monumentally important in the production of high-value chemicals.<sup>1</sup> The ability to perform selective oxidations in a synthetic lab also aids in the understanding of fundamental oxidative biological transformations.<sup>2</sup> However, most industrial-scale oxidations are nonselective, performed with strong, stoichiometric, environmentally hazardous oxidants, often under high heat and producing significant amounts of waste. As a result, the development of catalytic, environmentally friendly and selective oxidation methods has become one of the most important goals in oxidation chemistry.<sup>1,3-4</sup>

In an effort to develop such catalysts, chemists look to natural processes. Cytochrome P450 enzymes (CYP450s) are particularly relevant. CYP450s are named for their characteristic Soret band at 450 nm in the reduced state when complexed with CO.<sup>5</sup> These ubiquitous oxidative enzymes are found in most biological systems and some viruses.<sup>6</sup> In the human body, these enzymes perform biosynthesis of hormones and drug metabolism.<sup>7</sup> In general, CYP450s use molecular oxygen for their oxidations, transferring one oxygen to the substrate and reducing the second to water with biological reducing agents such as nicotinamide adenine dinucleotide (NADH).<sup>8</sup> The oxidations performed by CYP450s are characteristically chemo-, regio- and stereoselective, so the ability to replicate the reactivity of CYP450s is a valuable synthetic tool.<sup>9-10</sup>

The classical example of a stereospecific, chemospecific and regiospecific enzyme-catalyzed oxidation is that of camphor by CYP450<sub>cam</sub>, whose crystal structure is shown in Figure 1.<sup>11</sup> CYP450<sub>cam</sub> is the most well-characterized CYP450 enzyme, named

after its substrate, camphor. CYP450<sub>cam</sub> is found in *Pseudomonas putida*, a species of bacterium known for its ability to metabolize unusual substrates including camphor, caffeine and benzene. The ability of *P. putida* to metabolize these compounds is typically attributed to its powerful CYP450 monooxygenases.<sup>12</sup> In the case of camphor, the substrate is specifically hydroxylated to 5-*exo*-hydroxycamphor,<sup>11</sup> which is then metabolized to isobutyrate and acetate.<sup>13</sup> Benzene and toluene are oxidized to benzoate and toluate, which are further metabolized into Krebs cycle intermediates as well.<sup>12</sup> This reaction is chemospecific as only hydroxylation takes place, regiospecific as only C5 is oxidized and stereospecific as only the *exo* product is formed. This oxidation is outlined in Scheme 1.

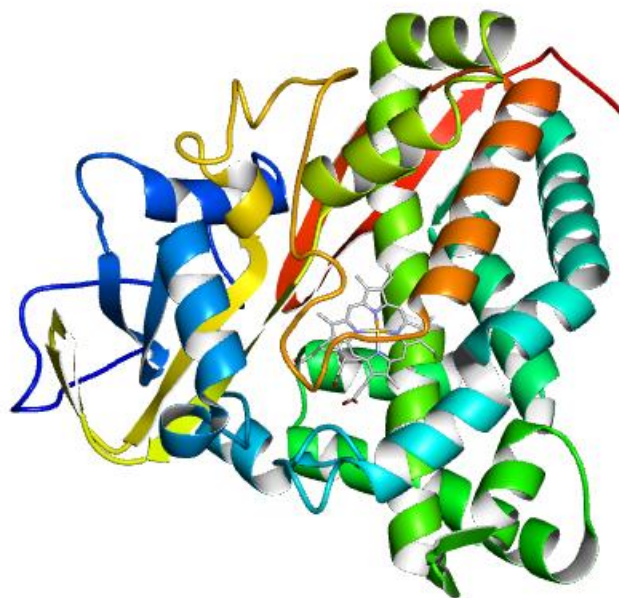
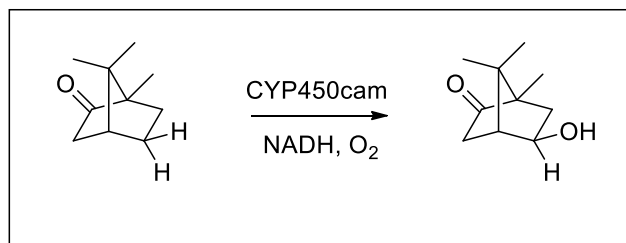


**Figure 1.** The crystal structure of CYP450<sub>cam</sub>.<sup>11</sup>



**Scheme 1.** The specific hydroxylation of camphor on C5, producing only the *exo* product.

CYP450s contain a heme *b* prosthetic group that acts as the active site, shown in Figure 2. A proximal cysteine ligand binds the octahedral iron(III) center, while a water molecule occupies the sixth position.<sup>13</sup> The water molecule is displaced by the substrate, followed by the binding of molecular oxygen and subsequent reduction of one oxygen to water. This results in an iron(IV)-oxo radical cation, termed Compound I.<sup>14</sup> Scheme 2 shows the catalytic cycle of CYP450s. Considering the catalytic abilities of these enzymes and the relative simplicity of the active site, the use of similar structures as biomimetic catalysts has garnered significant attention.<sup>15-16</sup> The active oxidant in the catalytic cycle of CYP450s is generally suggested to be Compound I.<sup>14, 17</sup> As such, high-valent metal-oxo species are particularly important intermediates in the catalytic cycles of biomimetic metalloporphyrins. Synthetic iron and manganese porphyrins have been investigated as biomimetic catalysts for a variety of oxygen atom transfer (OAT) reactions in past decades.<sup>18-19</sup> Scheme 3 illustrates typical oxidation reactions catalyzed by metalloporphyrins.<sup>15-16, 20-21</sup>

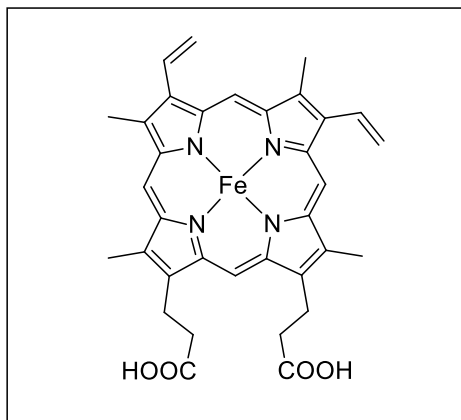
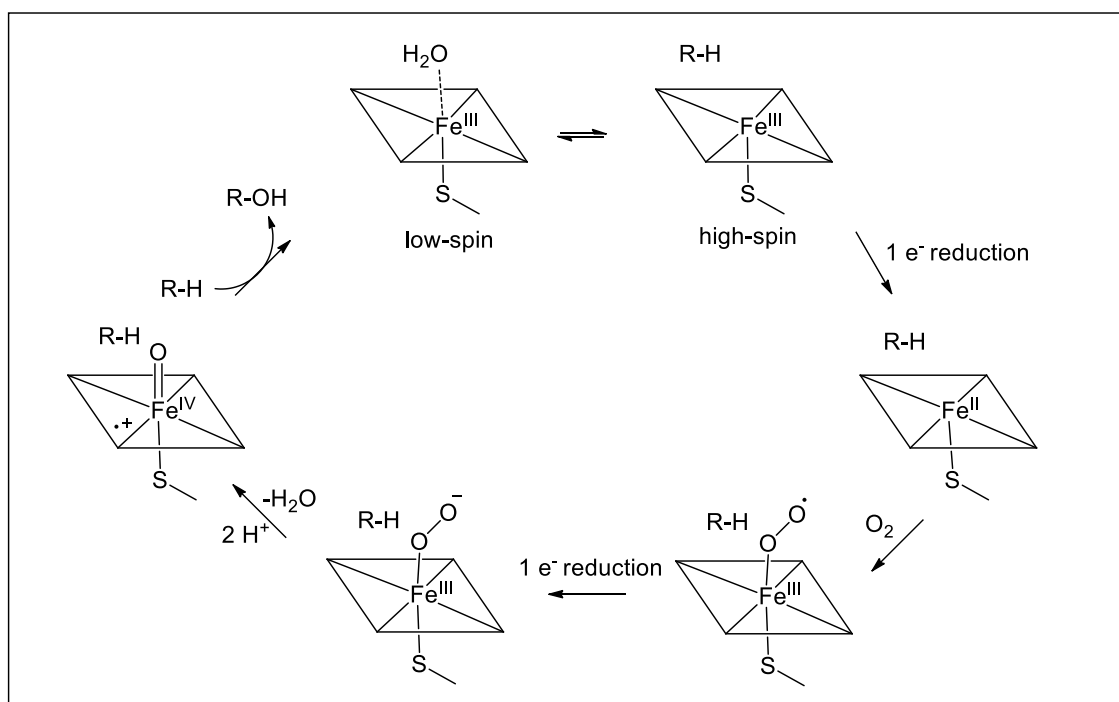
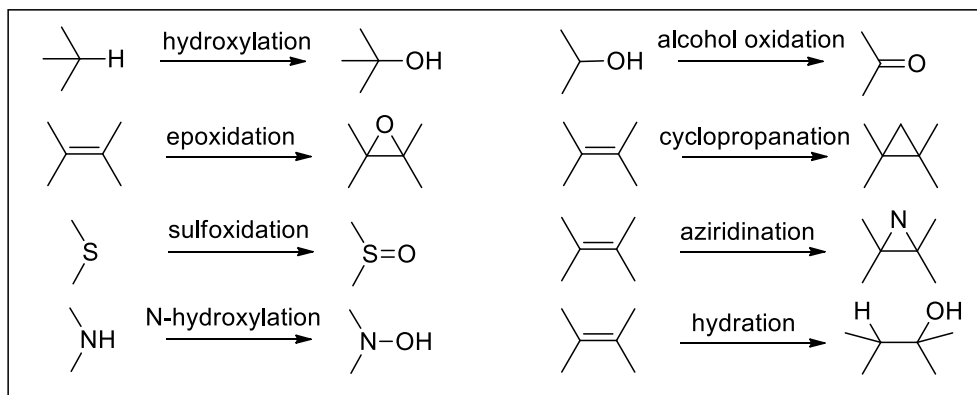


**Figure 2.** The structure of heme *b*, also called protoporphyrin IX.



**Scheme 2.** The catalytic cycle of CYP450 enzyme-catalyzed hydroxylation.





**Scheme 3.** Typical oxidations catalyzed by metalloporphyrins.

## 1.2 High-Valent Transition Metal-Oxo Species in Catalytic Oxidations

Because of their role in the catalytic cycle of CYP450s, high-valent transition metal-oxo species are of significant interest in the study of catalytic oxidations. High-valent metal-oxo species are typically considered the active oxidizing species in metalloporphyrin-mediated catalysis.<sup>22</sup> The first reported high-valent oxo-metalloporphyrin was an iron(IV) radical cation analogous to Compound I, later implicated in the catalytic cycle of CYP450s.<sup>13, 17, 23</sup> The detection of this complex was integral to the understanding of the catalytic cycle of CYP450s.<sup>14</sup> Since the detection of this first Compound I analogue in synthetic catalysts, the iron(IV) radical cation has been implicated as the major oxidizing intermediate in a variety of iron porphyrin-catalyzed oxidations.<sup>13, 16</sup>

The first high-valent manganese-oxo species was reported in 1980 by Groves et al.<sup>24</sup> Since the first report of a manganese(V)-oxo porphyrin, the development of metalloporphyrin catalysts with metals other than iron has increased. The study of high-valent manganese-oxo species is particularly interesting because iron(V)-oxo species have not been isolated in porphyrin systems, despite their proposed role in the catalytic

cycle of the enzymes.<sup>13</sup> A manganese(IV)-oxo porphyrin was also reported as an active oxidizing intermediate in the catalytic cycle of an electron-deficient porphyrin for the first time in 1987.<sup>25</sup> Since then, manganese(IV) and manganese(V)-oxo porphyrins have been implicated as the active oxidants in the catalytic cycles of a variety of porphyrin catalysts.<sup>18, 26</sup> Manganese(IV)-oxo radical cations have not been reported as active oxidants in the catalytic cycle of manganese porphyrins or corroles, although recently a manganese(IV)-hydroxy radical cation was characterized as a tautomer of a manganese(V)-oxo corrole formed by protonation of the oxo ligand.<sup>27</sup> Similar manganese(IV) radical cations have been characterized by addition of Lewis acids to the oxo ligand.<sup>28-30</sup>

### 1.3 Metalloporphyrins as Biomimetic Catalysts

The use of metalloporphyrins as oxidation catalysts began in 1979 when Groves et al. developed a tetraphenylporphyrinato iron(III) chloride complex and used it to catalyze the epoxidation of styrene and hydroxylation of cyclohexane.<sup>31</sup> An oxygen source is required to oxidize the original metalloporphyrin complex to its active high-valent metal-oxo intermediate. Groves et al. originally used iodosylbenzene (PhIO) as an oxygen source, but hydrogen peroxide ( $H_2O_2$ ), iodobenzene diacetate [ $PhI(OAc)_2$ ] and even molecular oxygen have been used as oxygen sources in later reports.<sup>4, 18, 32</sup> The choice of oxygen source is significant in that it can affect the reactivity and stability of the catalyst. Stronger oxidants, like iodosylbenzene and hydrogen peroxide, often result in faster formation of the high-valent metal-oxo species, but catalyst bleaching is increased as a result.<sup>33</sup> More recently, mild oxygen sources like iodobenzene diacetate have been used with metalloporphyrins to improve catalyst stability.<sup>18, 34</sup> Additionally,

environmental safety concerns have brought about the use of greener oxygen sources like hydrogen peroxide and molecular oxygen, whose only byproduct is water.<sup>32, 35</sup> Figure 3 shows the structure of common metalloporphyrin catalysts.<sup>36-38</sup> Manganese and ruthenium porphyrins are often studied because of their electronic similarity to iron coupled with the wide variety of available oxidation states in both metals. Manganese porphyrins in particular have recently been shown to efficiently and selectively catalyze epoxidations and sulfoxidations.<sup>18, 26</sup>

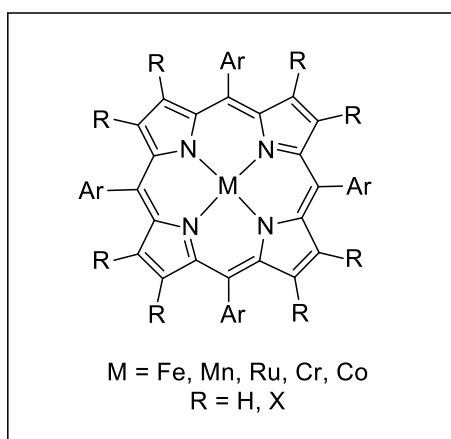


**Figure 3.** General structure of metalloporphyrin catalysts.

#### 1.4 Manganese Corroles as Biomimetic Catalysts

Corroles are 19-carbon aromatic structures analogous to porphyrins (Figure 4). The backbone is similar to that of corrin, the core structure of vitamin B12; the structures differ in that corrole is fully conjugated and aromatic.<sup>39</sup> The stability of corroles differs from that of porphyrins as corroles are prone to thermal degradation, contrasting the extremely stable porphyrin ligands. However, their high-valent metal complexes are significantly more stable than the analogous porphyrin metal complexes because of the trianionic nature of the corrole ligand.<sup>40</sup>

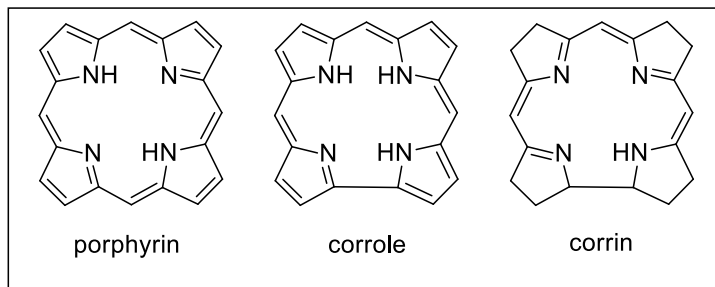
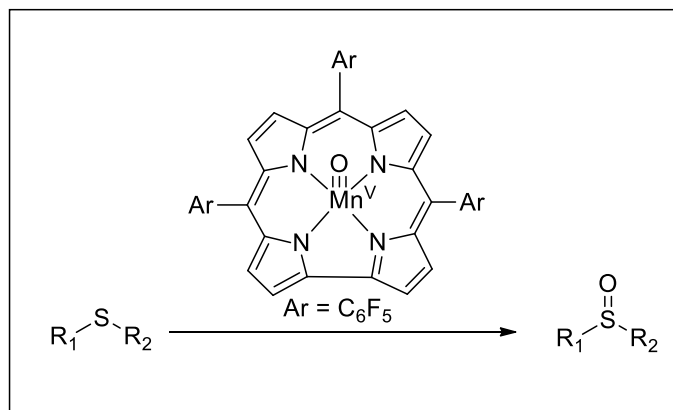


**Figure 4.** The structures of the porphyrin, corrole and corrin ligands.

The first corrole ligand was synthesized in 1965 by Johnson et al.<sup>41</sup> This difficult synthesis meant that the development of corrole catalysts was impractical for many years. In 1999, Gross et al. reported a facile, solvent-free synthesis of electron-poor corroles, and since then, the development of electron-poor metallocorrole catalysts has been an active field.<sup>42</sup> Metallocorroles have also been used in biochemical applications, as anticancer agents,<sup>43-48</sup> in antioxidant therapy<sup>49-50</sup> and in diabetic therapy.<sup>51</sup> The first report of metallocorrole catalysis appeared in 2000, when an iron(III) corrole was reported to be an effective catalyst towards epoxidation and cyclopropanation using iodosylbenzene as an oxygen source.<sup>52</sup> More recently, an oxo-manganese(V) complex of tris(pentafluorophenyl)corrole [Mn<sup>V</sup>(TPFC)O] was isolated as a relatively stable solid and used for stoichiometric sulfoxidations (Scheme 4).<sup>53</sup> This work aims to illustrate the efficacy of this corrole complex towards sulfoxidations and epoxidations under both catalytic and stoichiometric conditions.



**Scheme 4.** The oxidation of sulfides to sulfoxides with isolated Mn<sup>V</sup>TPFC(O).

### 1.5 Significance of Sulfoxidation Reactions

The selective oxidation of sulfides to sulfoxides without overoxidation to sulfones is of importance in the pharmaceutical industry.<sup>54</sup> Sulfoxides are commonly used in the production of antibacterial and antifungal compounds.<sup>55</sup> The problem of selective production of sulfoxides is most relevant in the synthesis of proton pump inhibitors, used to treat ulcers and heartburn.<sup>56</sup> Conventional methods for these oxidations involve the use of strong, stoichiometric oxidants, usually peroxyacids, or toxic heavy metal catalysts.<sup>57, 58</sup> Thus, environmentally-friendly sulfoxidation catalysis is a growing field.<sup>59</sup>

Manganese porphyrins and corroles have been shown to efficiently catalyze sulfoxidations.<sup>53</sup> Porphyrin catalysts typically exhibit high conversions, but the selectivities of the catalysts could be improved.<sup>18</sup> Corrole catalysts can exhibit greater selectivities, but their catalytic conversions suffer as a result.<sup>60</sup> In both cases, there are significant improvements to be made for more efficient catalytic methods. These difficulties extend to epoxidations by similar complexes.<sup>52</sup> There exists a demand for a

versatile catalyst that can selectively perform both sulfoxidations and hydroxylations under mild conditions with high product selectivities and turnover numbers.

## 2. EXPERIMENTAL SECTION

### 2.1 Materials

Solvents used for synthesis and column chromatography were used as received from Aldrich Chemical Co. without further purification, including acetone, dichloromethane, chloroform, acetonitrile, methanol, ethanol, diethyl ether, hexane and *N,N*-dimethylformamide (DMF). When used for kinetic and catalytic studies, these solvents were passed through a dry column of activated alumina (Grade I) to remove any water and impurities. Reactive substrates for kinetic and catalytic studies were also purchased from Aldrich Chemical Co. and purified before use via dry columns of activated alumina to remove impurities. These substrates include cyclohexene, *cis*-cyclooctene, ethylbenzene, styrene, *p*-chlorostyrene, *p*-fluorostyrene, *p*-methylstyrene, *p*-vinylanisole, thioanisole, *p*-chlorothioanisole, *p*-fluorothioanisole, *p*-methoxythioanisole and methyl *p*-tolyl sulfide. Pyrrole was freshly distilled immediately before use. Other reagents, including mesitaldehyde, pentafluorobenzaldehyde, benzaldehyde, boron trifluoride diethyl etherate (BF<sub>3</sub>·OEt<sub>2</sub>), 2,3-dichloro-5,6-dicyano-*p*-benzoquinone (DDQ), triethylamine, iodobenzene diacetate [PhI(OAc)<sub>2</sub>], hydrochloric acid (HCl), manganese(II) acetate tetrahydrate, chloroform-*d*, silver nitrate, tetrabutylammonium perchlorate (TBAP) and ferrocene, were used as received without further purification.

### 2.2 General Procedures

#### 2.2.1 Physical Measurements

UV-Visible absorption spectroscopy was performed on an Agilent 8453 diode array spectrophotometer. IR spectra were recorded using a Spectrum One FT-IR. <sup>1</sup>H-

NMR was performed on a JEOL ECA-500 MHz instrument with tetramethylsilane (TMS) as an internal standard. All chemical shifts are reported relative to TMS. Gas chromatography/mass spectrometry analyses were conducted with an Agilent GC 6890/MS 5973 equipped with a flame ionization detector (FID) and an autosampler. An Agilent J&W Cyclodex-B chiral capillary column was used for product analysis with 1,2,4-trichlorobenzene as an internal standard. Cyclic voltammetry was performed on a PARSTAT 2263 with a glassy carbon working electrode, a platinum wire counter electrode and an Ag/AgNO<sub>3</sub> reference electrode. Solutions of TBAP (0.1 M) and metal complex (1 mM) in acetonitrile were used for analysis.

### 2.2.2 Catalytic Oxidations

Unless otherwise specified, all catalytic reactions occurred in 0.5 mL of an anaerobic solvent, either dichloromethane, methanol or acetonitrile, with 1  $\mu$ mol catalyst, 0.2 mmol substrate and 0.3 mmol iodobenzene diacetate (1.5 equiv.) as an oxygen source. Catalysis with manganese corroles occurred in solutions in the absence of water, while catalysis with manganese porphyrin catalysts occurred in the presence of a small amount of water. Reactions were carried out at  $23 \pm 2^\circ\text{C}$ . Aliquots of the reaction mixtures were analyzed by GC/MS to determine the progress of the reaction as well as the ratios of products. Reactions were run at least twice; all data reported represents the average result of these runs.

## 2.3 Synthesis and Spectroscopic Characterization

### 2.3.1 Tris(pentafluorophenyl)corrole (H<sub>3</sub>TPFC, **1a**)

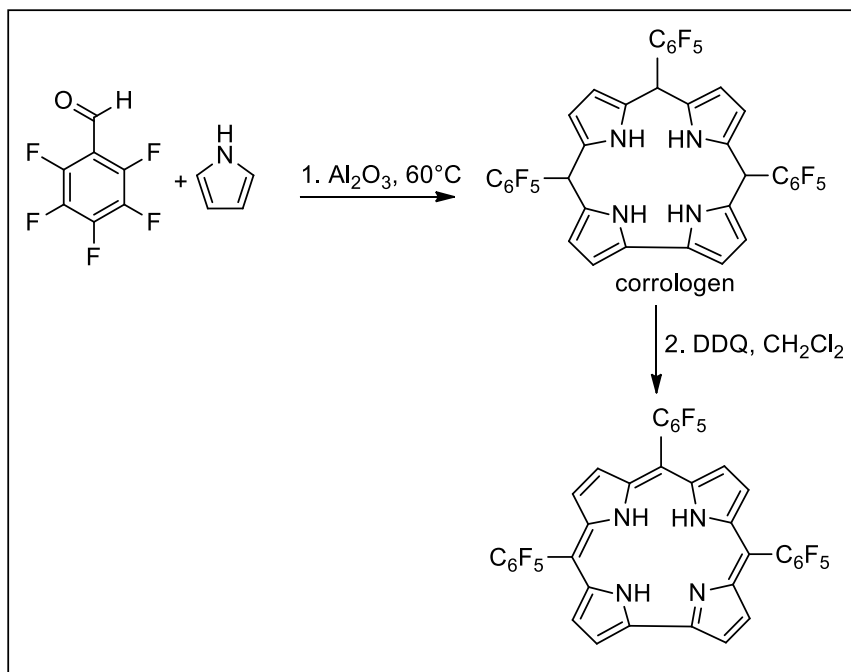
The synthesis of H<sub>3</sub>TPFC was performed according to the method described by Gross et al. in 1999,<sup>42</sup> shown in Scheme 5. Pentafluorobenzaldehyde (2.94 g, 15 mmol)



and distilled pyrrole (1.04 mL, 15 mmol) were dissolved in a small amount of CH<sub>2</sub>Cl<sub>2</sub> (ca. 2 mL). The mixture was added to a round-bottomed flask containing alumina (3 g) as a solid support. This mixture was heated to 60°C. After the CH<sub>2</sub>Cl<sub>2</sub> had completely evaporated, the mixture was allowed to react for 4 h, changing from colorless to dark brown. This first solvent-free condensation step forms the corrologen. Next, CH<sub>2</sub>Cl<sub>2</sub> (50 mL) was added to the tarry mixture, and the solution was stirred for about 10 min to dissolve. This solution was filtered under vacuum. The filtrate was collected and further reacted with 2,3-dichloro-5,6-dicyano-*p*-benzoquinone (DDQ, 1.7 g, 7.5 mmol, 2 equiv.) in a one-electron oxidation for 1 h that completed the aromatic system. Reaction progress was monitored using thin layer chromatography (TLC). A purple band was seen with strong fluorescence under UV light. If left at ambient temperature for several hours, this band turned green. The band represented the desired corrole product.

The product was isolated on a series of normal-phase columns with silica gel (SiO<sub>2</sub>). First, the tarry portion of the product mixture was separated from the rest of the products using a fairly short (4-5 inches) column with a mixture of dichloromethane and hexane (1:3 v/v) as the eluent. All products were collected from this column, while the tarry, insoluble impurities were removed. The desired product was isolated in an additional column. This column was much longer (8-9 inches) with dichloromethane and hexane (1:6 v/v) as the eluent. A purple band that strongly fluoresced under UV light was collected. The product and its purity were analyzed using <sup>1</sup>H-NMR, and a third column was performed as needed for further purification. The final product was characterized by <sup>1</sup>H-NMR (Figure 5) and UV-vis (Figure 6) spectroscopies, matching literature reports.<sup>42, 61</sup>

H<sub>3</sub>TPFC (**1a**) Yield% = 5% (145 mg). <sup>1</sup>H-NMR (500 MHz, CDCl<sub>3</sub>) δ (ppm): -2.25 (s, 3H, N-H), 8.65 (4H), 8.75 (2H), 9.12 (2H). UV-Vis (CH<sub>2</sub>Cl<sub>2</sub>) λ<sub>max</sub> (nm): 408, 560, 600.



**Scheme 5.** The two-step synthesis of H<sub>3</sub>TPFC (**1a**).

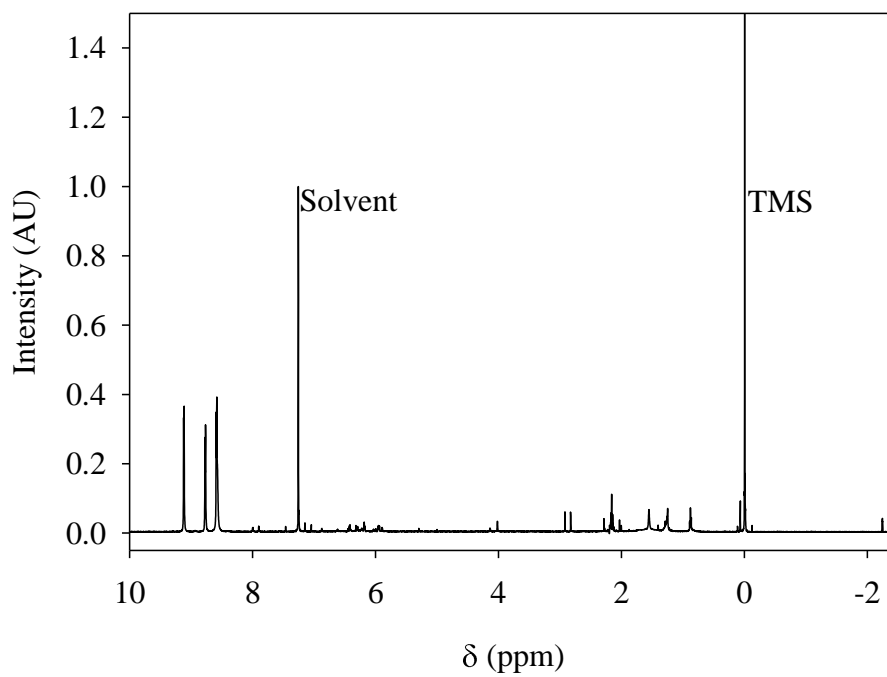


**Figure 5.** The <sup>1</sup>H-NMR spectrum of H<sub>3</sub>TPFC (**1a**) in CDCl<sub>3</sub>.

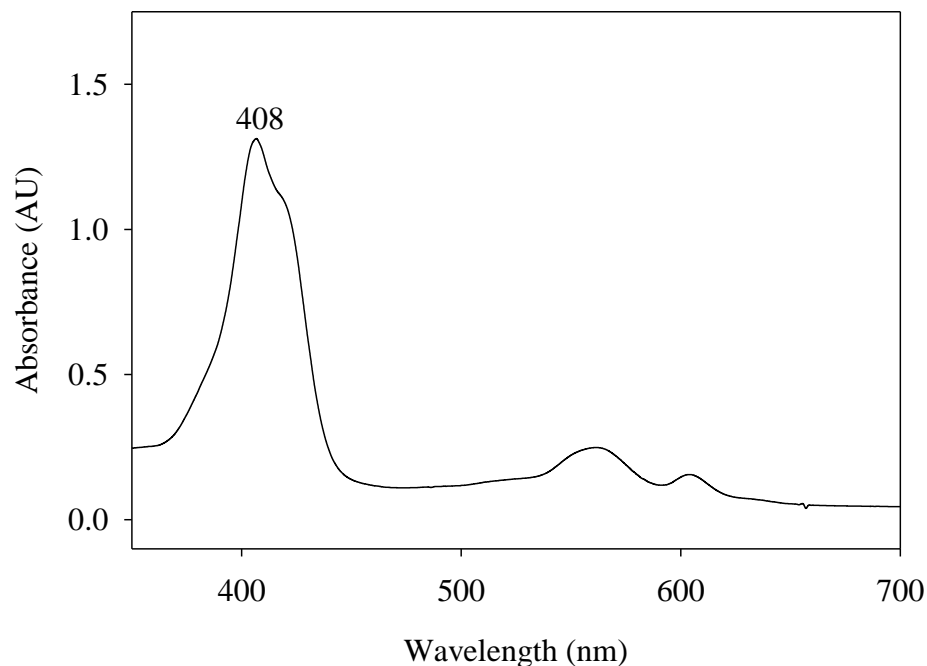


**Figure 6.** The UV-visible absorption spectrum of H<sub>3</sub>TPFC (**1a**) in CH<sub>2</sub>Cl<sub>2</sub>.

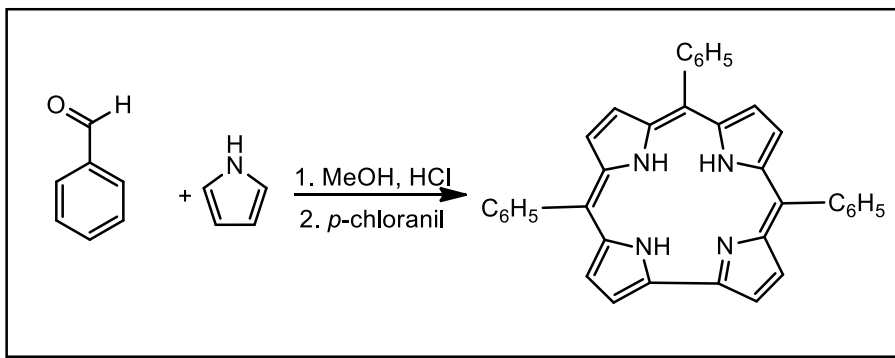
### 2.3.2 Triphenylcorrole (H<sub>3</sub>TPC, **1b**)

This corrole was prepared based on the report of Koszarna and Gryko in 2006,<sup>62</sup> as shown in Scheme 6. Benzaldehyde (510  $\mu$ L, 5 mmol), freshly distilled pyrrole (700  $\mu$ L, 10 mmol) and 500 mL of methanol were mixed in a 1 L round-bottomed flask. The solution was degassed with argon for 5 min. To start the reaction, concentrated hydrochloric acid was added as the catalyst; the mixture was stirred for 3 h and monitored by TLC. The resulting mixture was extracted with CHCl<sub>3</sub> (100 mL) three times, and the remaining organic layer was then washed with DI water to remove residual acid. The resulting solution was then dried with sodium sulfate. *p*-Chloranil (1.23 g, 5 mmol) was added and the mixture was refluxed for 1 h, monitored by TLC. The resulting mixture was purified on a column of silica gel and eluted with dichloromethane to yield a brown-green solid product. This product was characterized

with  $^1\text{H-NMR}$  and UV-vis, shown in Figures 7 and 8, respectively, matching literature-reported spectra.<sup>62</sup>

$\text{H}_3\text{TPC}$  (**1b**) Yield% = 7% (80 mg).  $^1\text{H-NMR}$  (500 MHz,  $\text{CDCl}_3$ )  $\delta$  (ppm): -2.90 (3H, N-H), 7.73-7.83 (9H), 8.17 (2H), 8.38 (4H), 8.55 (2H), 8.60 (2H), 8.87 (2H), 8.95 (2H).

UV-Vis ( $\text{CH}_2\text{Cl}_2$ )  $\lambda_{\text{max}}$  (nm): 415, 568, 615.



**Scheme 6.** The synthesis of  $\text{H}_3\text{TPC}$  (**1b**).

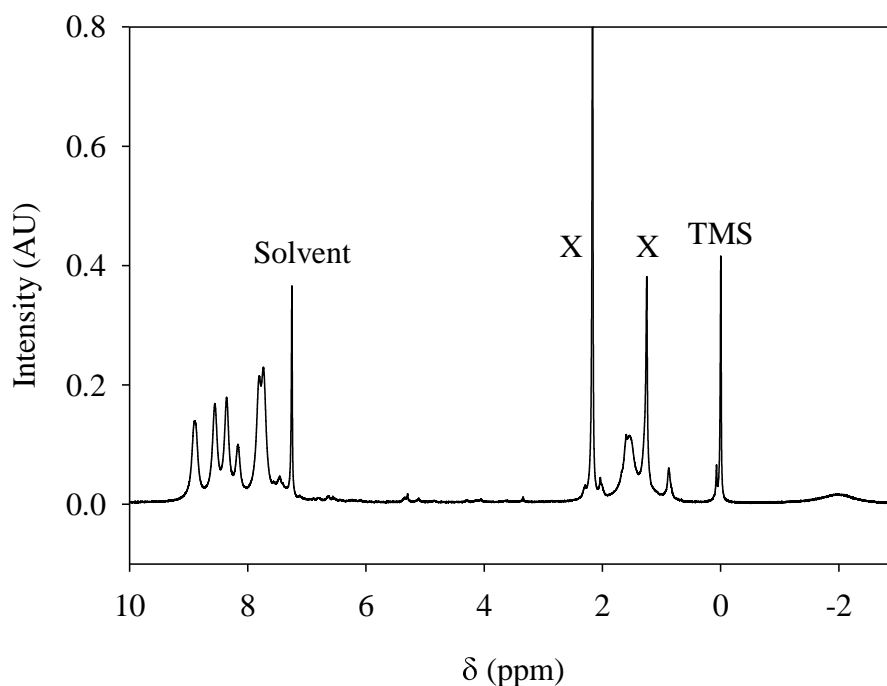


**Figure 7.** The  $^1\text{H-NMR}$  spectrum of  $\text{H}_3\text{TPC}$  (**1b**).

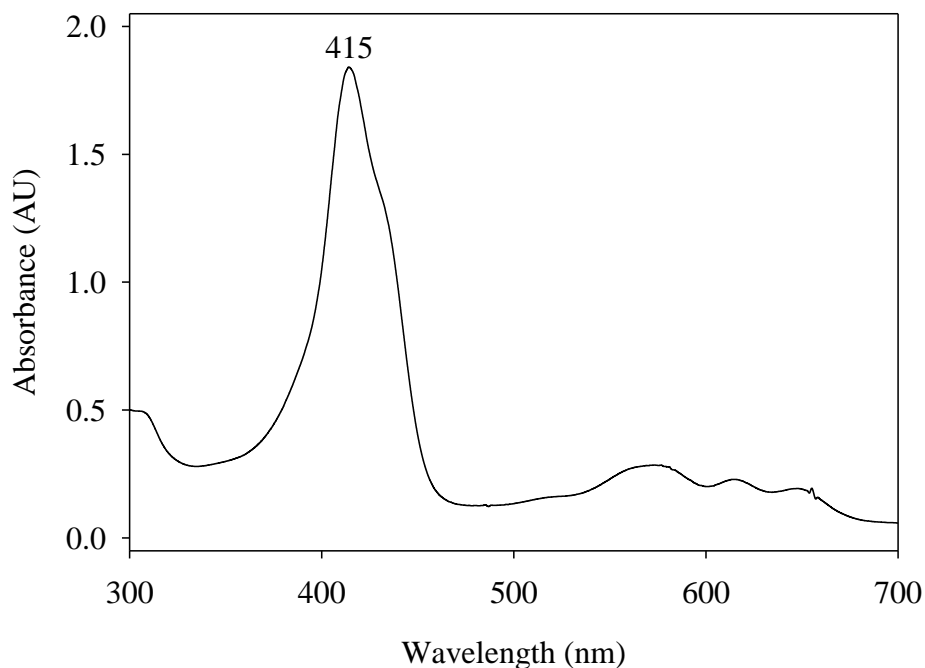


**Figure 8.** The UV-visible absorption spectrum of H<sub>3</sub>TPC (**1b**).

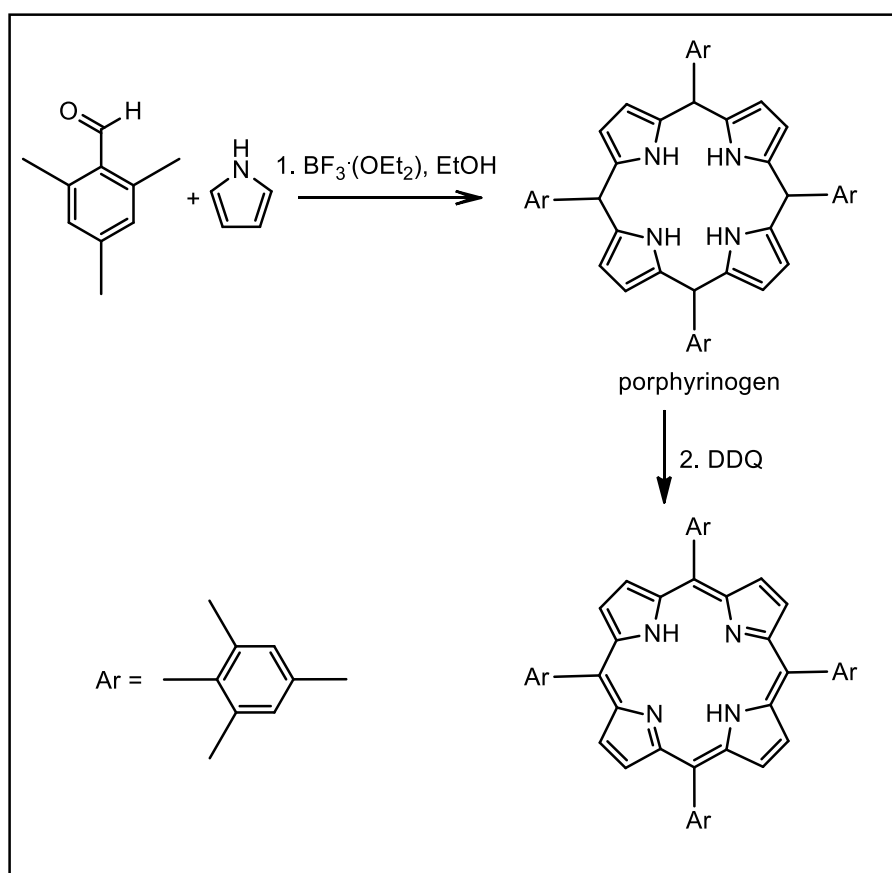
### 2.3.3 *meso*-Tetramesitylporphyrin (H<sub>2</sub>TMP, **1c**)

This free porphyrin ligand was synthesized according to the method reported by Lindsey et al.,<sup>63</sup> shown in Scheme 7. Mesitaldehyde (736  $\mu$ L, 5 mmol), distilled pyrrole (347  $\mu$ L, 5 mmol) and ethanol (3.47 mL, 0.5% v/v) were dissolved in chloroform (500 mL) in a 1L round-bottomed flask, and the mixture was degassed under argon for 5 min. Boron trifluoride diethyl etherate (BF<sub>3</sub>·OEt<sub>2</sub>, 660  $\mu$ L, 1.65 mmol) was added in a dropwise manner, and the solution was stirred at room temperature for 1 h. The BF<sub>3</sub>·OEt<sub>2</sub> and ethanol act as co-catalysts for the condensation step, forming the porphyrinogen. This step of the synthesis was monitored using UV-visible spectroscopy, as the intermediate product shows a distinctive band at 480 nm.

To complete the formation of the porphyrin, the porphyrinogen solution was refluxed with an excess of DDQ (1.36 g, 6 mmol) for 1 h. This one-electron oxidation process was again monitored using UV-visible spectroscopy. Triethylamine (920  $\mu$ L, 6.6

mmol) was added after the reflux to quench the highly acidic solution. The solvent was evaporated, and the crude product was washed with methanol under vacuum until the filtrate became clear. The bright purple product was further purified using a column of silica gel with dichloromethane as the eluent. The product was characterized with UV-visible spectroscopy and  $^1\text{H-NMR}$ , shown in Figures 9 and 10, respectively, matching the literature.<sup>63</sup>

$\text{H}_2\text{TMP}$  (**1c**) Yield = 18% (185 mg).  $^1\text{H-NMR}$  (500 MHz,  $\text{CDCl}_3$ )  $\delta$  (ppm): -2.50 (2H, N-H), 1.81 (24H, *o*- $\text{CH}_3$ ), 2.62 (12H, *p*- $\text{CH}_3$ ), 7.25 (8H, *m*-H), 8.61 (8H, pyrrolic). UV-Vis ( $\text{CH}_2\text{Cl}_2$ )  $\lambda_{\text{max}}$  (nm): 416, 440, 516.



**Scheme 7.** The synthesis of  $\text{H}_2\text{TMP}$  (**1c**).

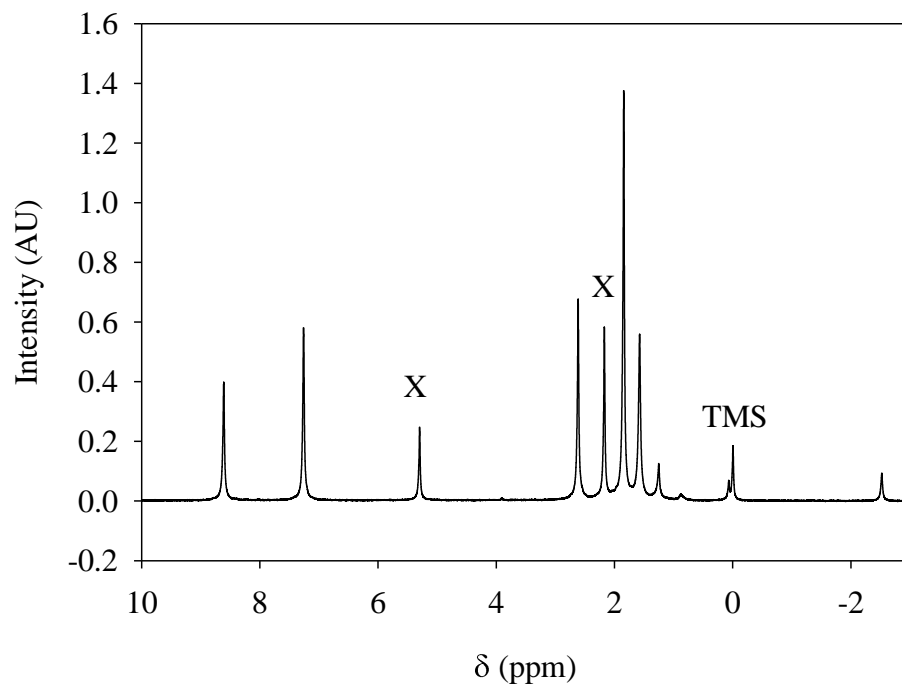


**Figure 9.** The <sup>1</sup>H-NMR spectrum of H<sub>2</sub>TMP (**1c**).

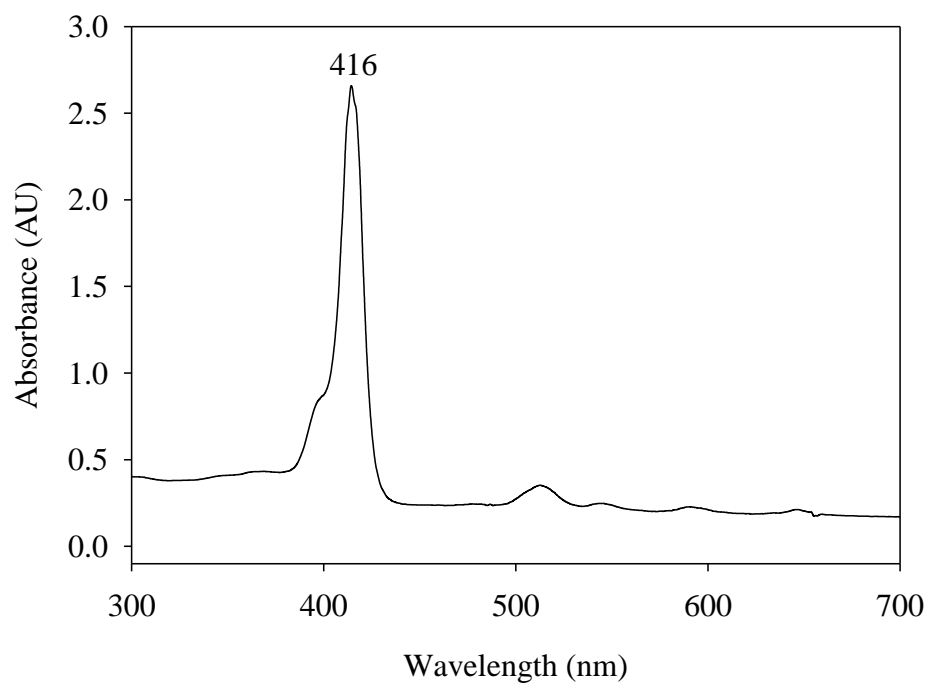


**Figure 10.** The UV-visible absorption spectrum of H<sub>2</sub>TMP (**1c**).

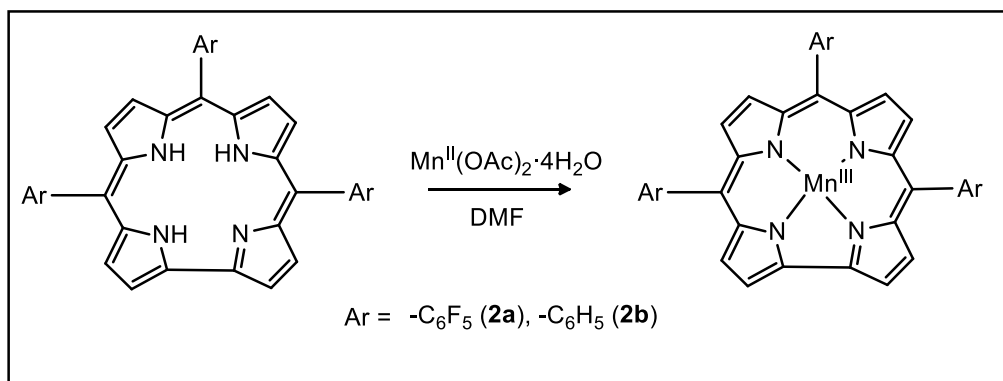
### 2.3.4 Manganese(III) Corroles [Mn<sup>III</sup>Cor·(OEt<sub>2</sub>)<sub>2</sub>, **2**]

The insertion of manganese into the corrole ligands was achieved by a reflux of the free ligand with manganese(II) acetate tetrahydrate in DMF, shown in Scheme 8. Free-base corrole (100 mg) and a large excess of Mn<sup>II</sup>(OAc)<sub>2</sub>·4H<sub>2</sub>O (200 mg) were dissolved in DMF (50 mL) in a round-bottomed flask fitted with a reflux condenser. The solution was refluxed for 1 h, and reaction progress was monitored by TLC.

After reflux, DMF was removed by rotary evaporation. The crude, solid product was purified by a column of silica gel with diethyl ether as the eluent. The pure product was isolated as a dark green band. Both products were characterized by UV-vis and <sup>1</sup>H-NMR spectroscopies with **2a** spectra shown in Figures 11 and 12. **2b** spectra are shown in Figures 13 and 14. As expected for paramagnetic complexes, the <sup>1</sup>H-NMR spectra of **2a** and **2b** are characterized by an unusually large chemical shift range and exceptionally broad peaks.

Mn<sup>III</sup>TPFC·(OEt<sub>2</sub>)<sub>2</sub> (**2a**) Yield% = 88% (97 mg). <sup>1</sup>H-NMR (500 MHz, CDCl<sub>3</sub>) δ (ppm): -23.82, -4.16, 1.04, 3.17, 8.34, 10.80. UV-Vis (CH<sub>2</sub>Cl<sub>2</sub>) λ<sub>max</sub> (nm): 418, 484, 602.

Mn<sup>III</sup>TPC·(OEt<sub>2</sub>)<sub>2</sub> (**2b**) Yield% = 90% (102 mg). <sup>1</sup>H-NMR (500 MHz, CDCl<sub>3</sub>) δ (ppm): -29.93, -1.79, 1.43, 7.68, 14.28, 15.27–17.29. UV-Vis (CH<sub>2</sub>Cl<sub>2</sub>) λ<sub>max</sub> (nm): 313, 430.



**Scheme 8.** Synthesis of manganese(III) corrole complexes.



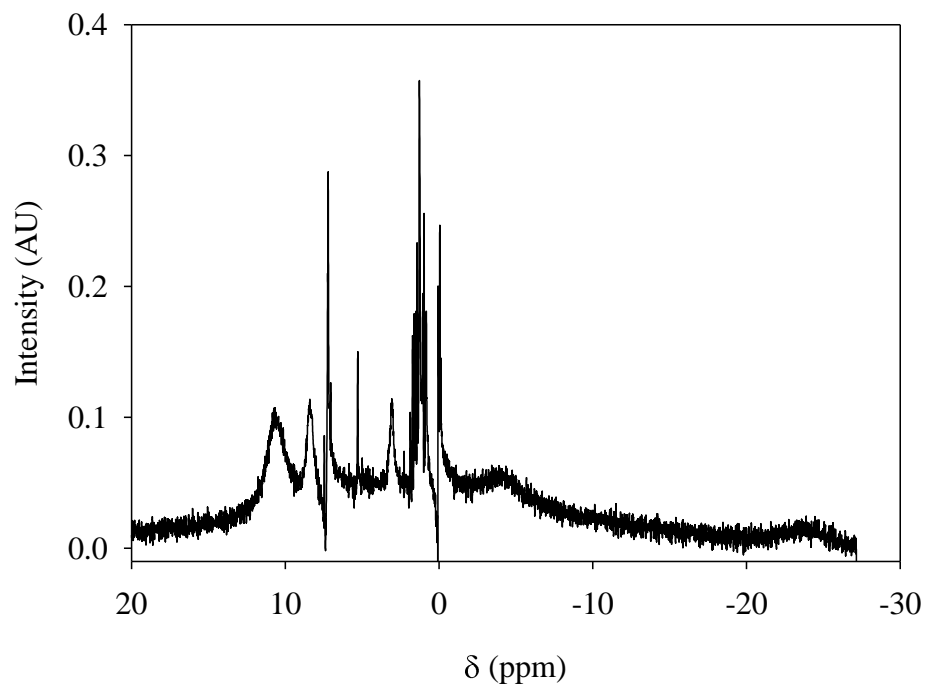


**Figure 11.** The  $^1\text{H}$ -NMR spectrum of **2a** in  $\text{CDCl}_3$ .

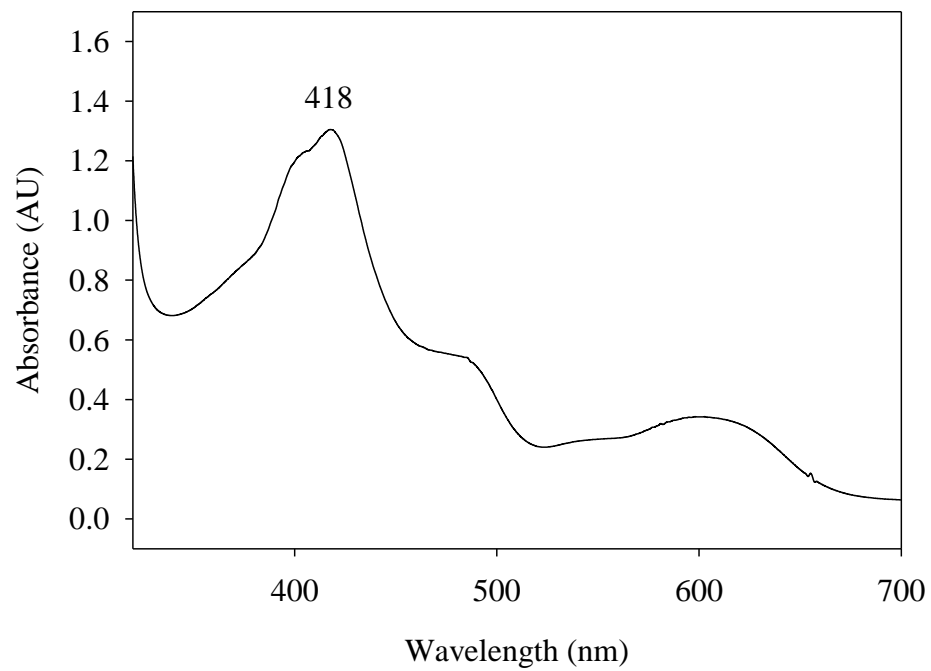


**Figure 12.** The UV-visible absorption spectrum of **2a** in  $\text{CH}_2\text{Cl}_2$ .

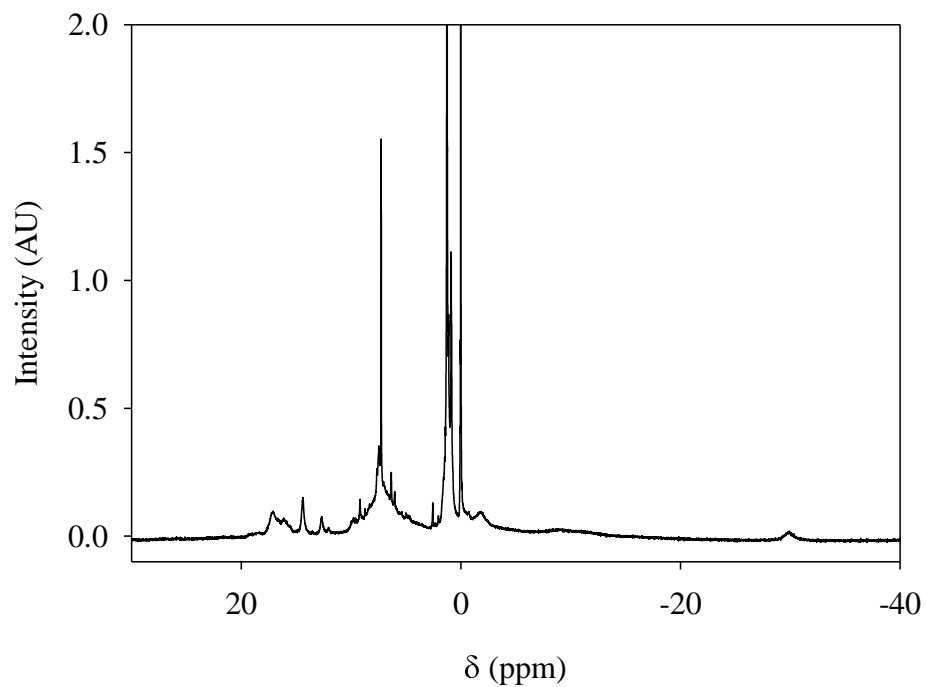


**Figure 13.** The <sup>1</sup>H-NMR spectrum of **2b** in CDCl<sub>3</sub>.

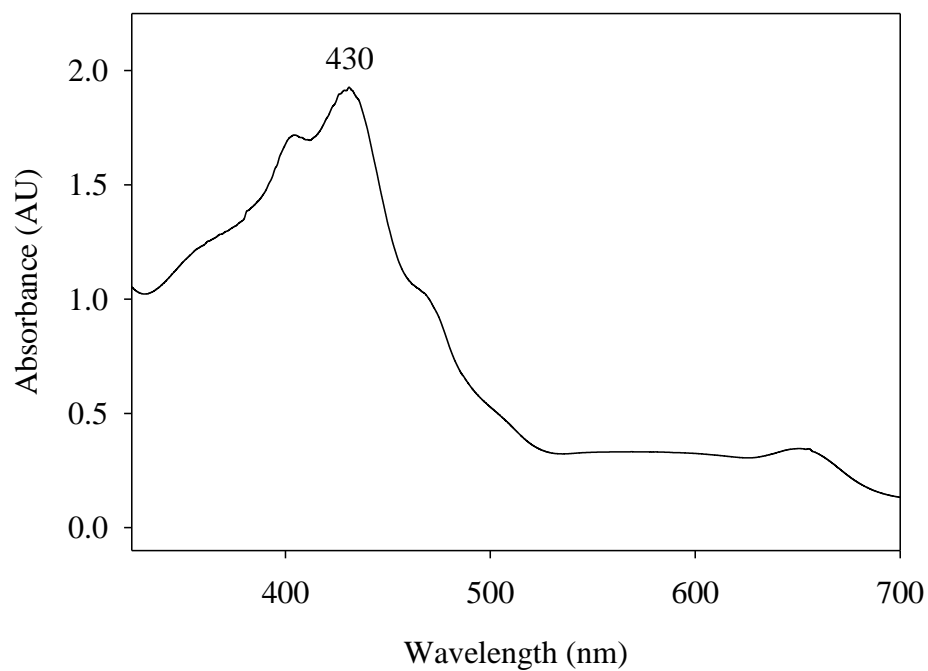


**Figure 14.** The UV-visible absorption spectrum of **2b** in CH<sub>2</sub>Cl<sub>2</sub>.

### 2.3.5 Manganese(III) Porphyrin Chloride [ $\text{Mn}^{\text{III}}(\text{TMP})\text{Cl}$ , **2c**]

The synthesis of the manganese(III) porphyrin is similar to that of the manganese(III) corroles. The free ligand (100 mg) and a large excess of  $\text{Mn}^{\text{II}}(\text{OAc})_2 \cdot 4\text{H}_2\text{O}$  (300 mg) were dissolved in DMF (50 mL) in a 100 mL round-bottomed flask fitted with a reflux condenser. This solution was degassed for 5 min under argon, then refluxed for 1 h. Reaction progress was monitored by TLC.

After reflux, the DMF was removed by rotary evaporation, and the crude product was dissolved in dichloromethane (50 mL). This solution was mixed with hydrochloric acid (6 M, 50 mL) in order to exchange the axial ligand from hydroxy to chloride. The solution was extracted with dichloromethane (50 mL) three times. The remaining organic layer was then washed with DI water (50 mL) three times and dried with sodium sulfate. The solvent was evaporated and the desired product was purified in a column of silica gel and eluted with a mixture of dichloromethane and hexane (1:1 v/v). The pure product was isolated as a bright green band and characterized by  $^1\text{H}$ -NMR and UV-vis in Figure 15 and Figure 16, respectively. The manganese(III) porphyrin complex is paramagnetic, consistent with its broad  $^1\text{H}$ -NMR spectrum.

$\text{Mn}^{\text{III}}(\text{TMP})\text{Cl}$  (**2c**) Yield%= 92% (105 mg).  $^1\text{H}$ -NMR (500 MHz,  $\text{CDCl}_3$ )  $\delta$  (ppm): -21.2, 1.31, 2.63, 7.57–8.94. UV-Vis ( $\text{CH}_2\text{Cl}_2$ )  $\lambda_{\text{max}}$  (nm): 375, 480, 585, 623.

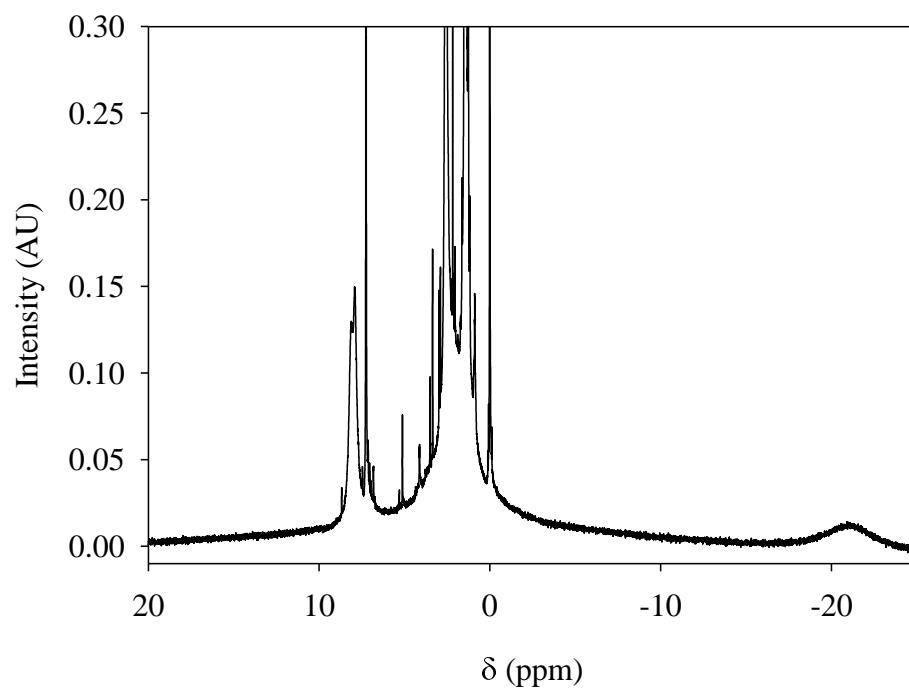


**Figure 15.** The  $^1\text{H-NMR}$  spectrum of **2c** in  $\text{CDCl}_3$ .

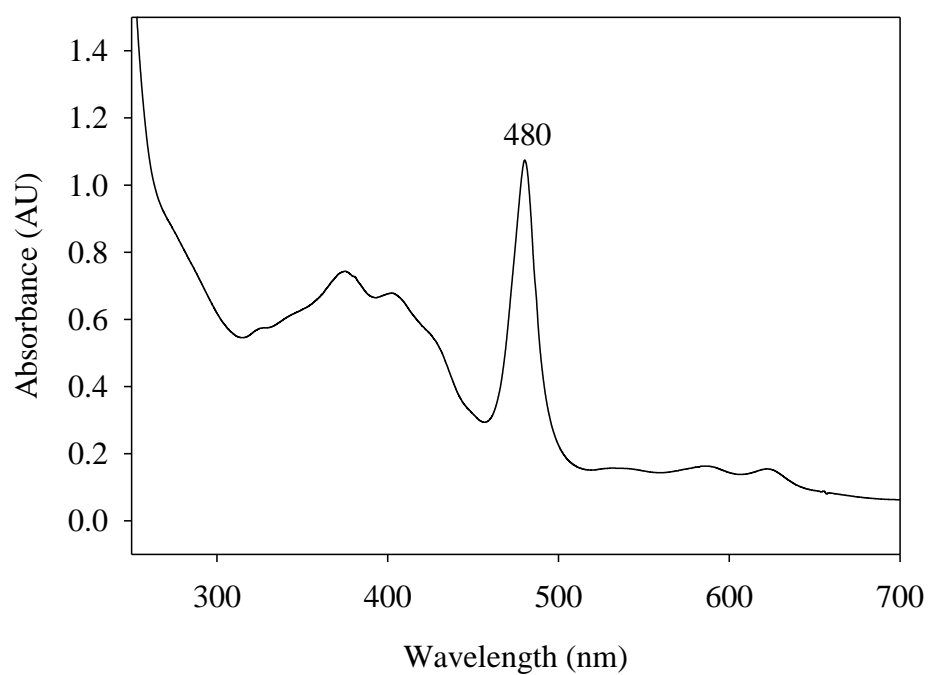


**Figure 16.** The UV-visible absorption spectrum of **2c** in  $\text{CH}_2\text{Cl}_2$ .

### 3. KINETIC STUDIES OF STOICHIOMETRIC OXIDATIONS BY $\text{Mn}^{\text{V}}(\text{TPFC})\text{O}$ AND $\text{Mn}^{\text{IV}}(\text{TMP})\text{O}$

#### 3.1 Introduction

Manganese porphyrins and corroles are among the most widely used oxygen atom transfer (OAT) catalysts because of the wide variety of available oxidation states that are accessible to manganese complexes. High-valent metal-oxo species are fundamentally important due to the roles they play in catalytic OAT mechanisms. Identification of the active metal-oxo complex is decidedly complicated, as disproportionation and comproportionation mechanisms can allow for the active species to be generated in nearly undetectable amounts. This holds true for manganese(V)-oxo corroles, whose isolated forms are reported to be inactive towards olefins, despite their known catalytic activity in solution. Manganese corroles have been shown to efficiently perform stoichiometric sulfoxidations, with evidence of a multiple-pathway mechanism of oxidation that depends on the electron-rich or poor nature of the corrole ligand. This work reports that a single corrole system can access multiple pathways of the mechanism depending on the solvent used.

#### 3.2. Results and Discussion

##### 3.2.1 Electrochemical Studies

Cyclic voltammetry was used to characterize and compare the oxidation potentials of **2a** and **2b**. These voltammograms are shown in Figures 17 and 18, respectively. The oxidation of ferrocene under the same conditions gave  $E_{1/2} = 85$  mV. Notably, the potential at the cathodic and anodic peaks differs by less than 80 mV for both **2a** and **2b**, clearly indicating a one-electron oxidation from manganese(III) to manganese(IV) in both systems. Figure 19 shows a linear Cottrell plot<sup>64</sup> of peak current

versus the square root of the scan rate for **2a**, verifying that the process observed is diffusion-controlled.

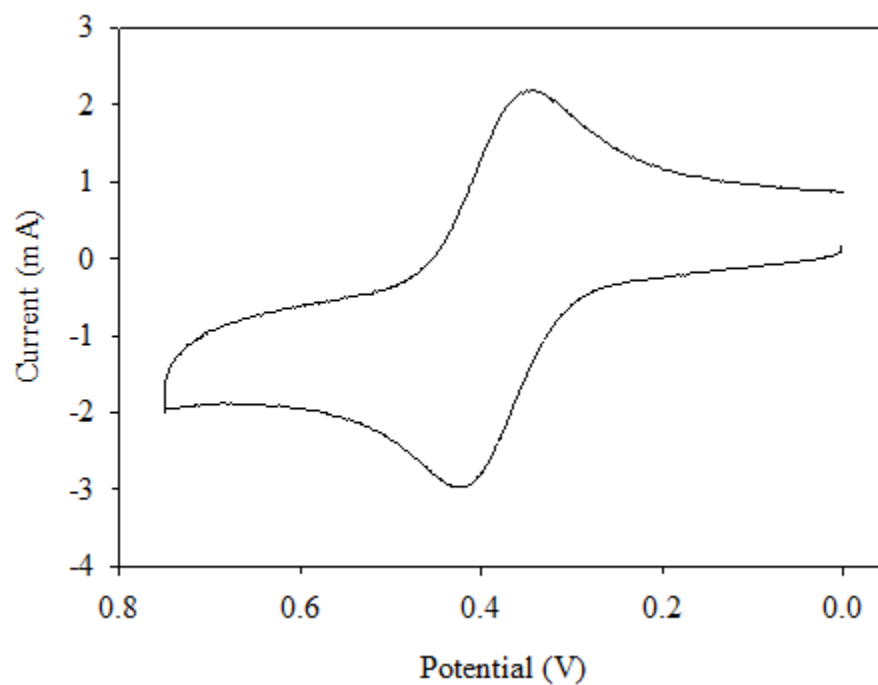


**Figure 17.** A cyclic voltammogram of **2a** (1 mM) in a 0.1 M TBAP/CH<sub>3</sub>CN solution at scan rate 100 mV/s and with a three-electrode system: a glassy carbon working electrode, a platinum wire counter electrode and an Ag/AgNO<sub>3</sub> reference electrode. The  $E_{1/2}$  of the system under these conditions is 385 mV.

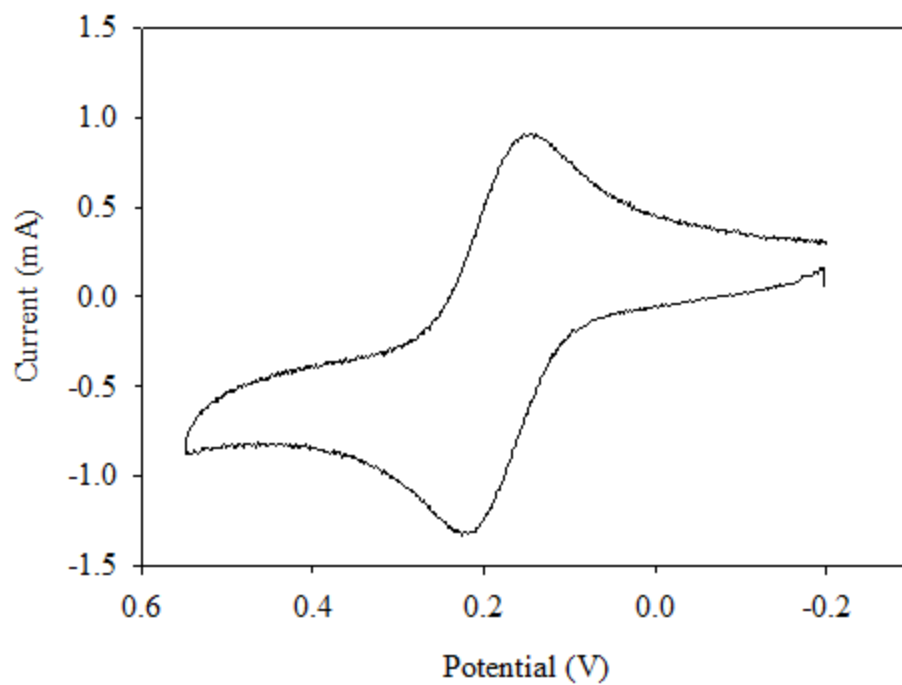


**Figure 18.** A cyclic voltammogram of **2b** (1 mM) in a 0.1 M TBAP/CH<sub>3</sub>CN solution at scan rate 100 mV/s with a three-electrode system: a glassy carbon working electrode, a platinum wire counter electrode and a Ag/AgNO<sub>3</sub> reference electrode. The  $E_{1/2}$  of the system under these conditions is 186 mV.

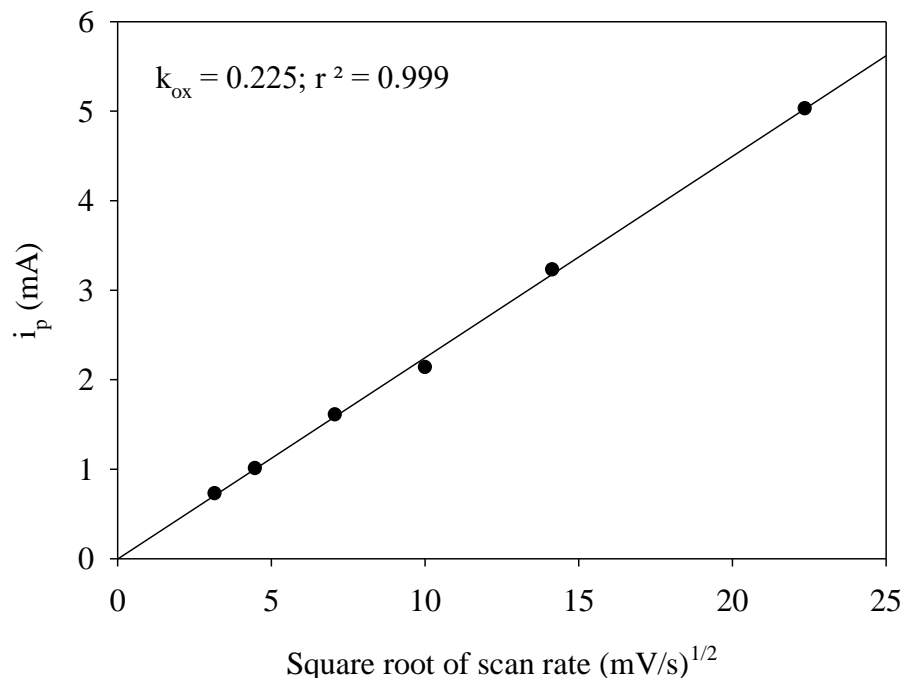


**Figure 19.** A Cottrell plot of the peak current of the oxidation of **2a** at varied scan rates. This plot is linear for diffusion-controlled electrochemical systems, and  $k_{\text{ox}}$  is a collection of constants specific to the system.

The relative oxidation potentials of **2a** and **2b** can be explained by the electron-demanding nature of the TPFC ligand. Upon oxidation of **2a**, the resulting manganese(IV) species is more destabilized, so it becomes much more difficult to perform this oxidation. This also implies that the oxidizing power of a high-valent metal-oxo species with a more electron-demanding corrole ligand is stronger than that of a non-electron deficient ligand in view of the electrophilic nature of the high-valent manganese-oxo species.

### 3.2.2 Solvent Effect

In previous work by Kumar et al., the reactivity of isolated  $\text{Mn}^{\text{V}}(\text{TPFC})\text{O}$  (**3a**) towards OAT in ethyl acetate was explored.<sup>53</sup> This work, however, aims to explore the



effects of differing solvents on the reactivity and the reaction pathways of **3a**. To determine the appropriate solvent for our experiments, the stability of **3a** was first examined in each of the chosen solvents: dichloromethane, acetonitrile, methanol and chloroform. **3a** was generated *in situ* in 2 mL of the chosen solvent from the corresponding precursor **2a** ( $2.5 \times 10^{-5}$  M) using *m*-CPBA (3 equiv.) as a sacrificial oxidant. *m*-CPBA was chosen because of its oxidizing power with the metallocorrole. The generation of **3a** was verified using time-resolved UV-vis spectra over 40 s, as the spectrum for **3a** is well-characterized in the literature.<sup>53</sup> For comparison, the stability of  $\text{Mn}^{\text{IV}}(\text{TMP})\text{O}$  (**4c**) in various solvents was also studied. **4c** was generated from its precursor **2c** ( $1.8 \times 10^{-5}$  M) in 2.0 mL solvent with  $\text{PhI}(\text{OAc})_2$  (10 equiv.) as the sacrificial oxidant.  $\text{PhI}(\text{OAc})_2$  was chosen instead of *m*-CPBA because of its mild oxidizing ability, which allows for the formation of a manganese(IV)-oxo instead of a manganese(V)-oxo porphyrin. This is attributed to the comproportionation of the manganese(III) precursor and the manganese(V)-oxo species into a manganese(IV)-oxo species. Figure 20 shows the UV-vis spectra of **3a** and **4c** in  $\text{CH}_3\text{CN}$ .

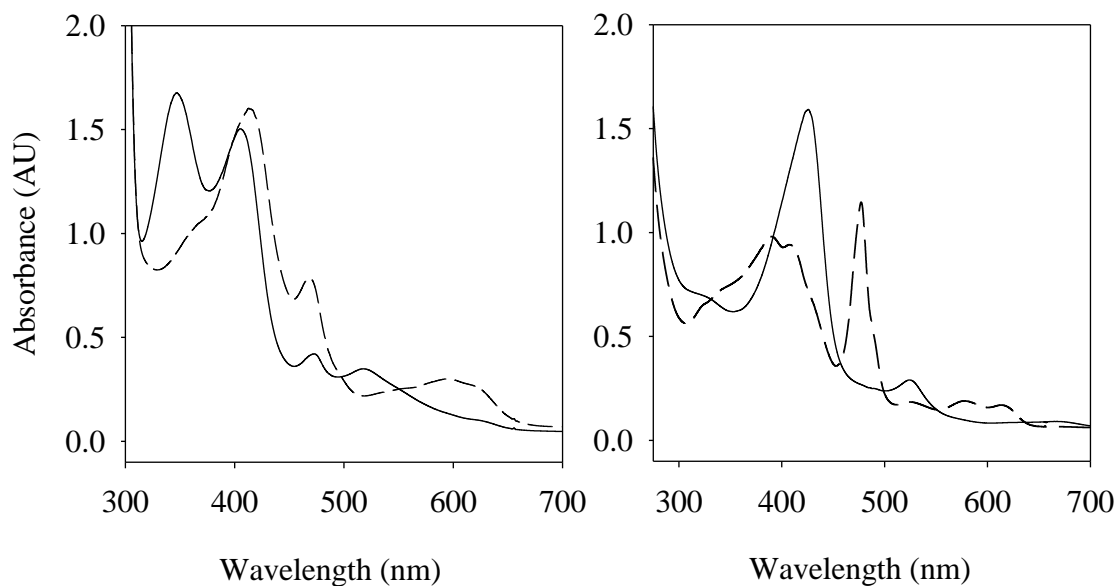


**Figure 20.** The UV-visible absorption spectra of **3a** (left, solid line) generated by oxidation of **2a** (left, dashed line) with *m*-CPBA in CH<sub>3</sub>CN and **4c** (right, solid line) generated by oxidation of **2c** (right, dashed line).

**3a** was initially expected to regenerate **2a** over time, as is expected under catalytic conditions to allow regeneration of the catalyst. In CH<sub>3</sub>CN, that is the case; Figure 21 shows time-resolved spectra of **3a** decaying into **2a** over the course of 3 h in CH<sub>3</sub>CN, with an observed pseudo-first-order rate constant of  $k_{\text{obs}} = 4.2 \times 10^{-5} \text{ s}^{-1}$ . This decay is signaled by a decreased intensity at 349 nm as well as a distinctive peak forming at 465 nm. This is similar to previously-reported results with ethyl acetate as the solvent.<sup>53</sup> However, in both CH<sub>2</sub>Cl<sub>2</sub> and CHCl<sub>3</sub>, a suspected Mn<sup>IV</sup>(TPFC)X species was observed. The identification of this species as a manganese(IV) is based on reported manganese(IV) corroles generated by Laser Flash Photolysis (LFP) studies.<sup>65</sup> Figure 22 shows the decay of **3a** to Mn<sup>IV</sup>(TPFC)X in CH<sub>2</sub>Cl<sub>2</sub> over 5 h, with  $k_{\text{obs}} = 2.0 \times 10^{-5} \text{ s}^{-1}$ , monitored at 349 nm. To fully investigate the kinetics of OAT by **3a**, reactions were

studied in both  $\text{CH}_2\text{Cl}_2$  and  $\text{CH}_3\text{CN}$ .  $\text{CH}_2\text{Cl}_2$  was chosen because of the longer lifetime of **3a** compared to that in  $\text{CHCl}_3$ .

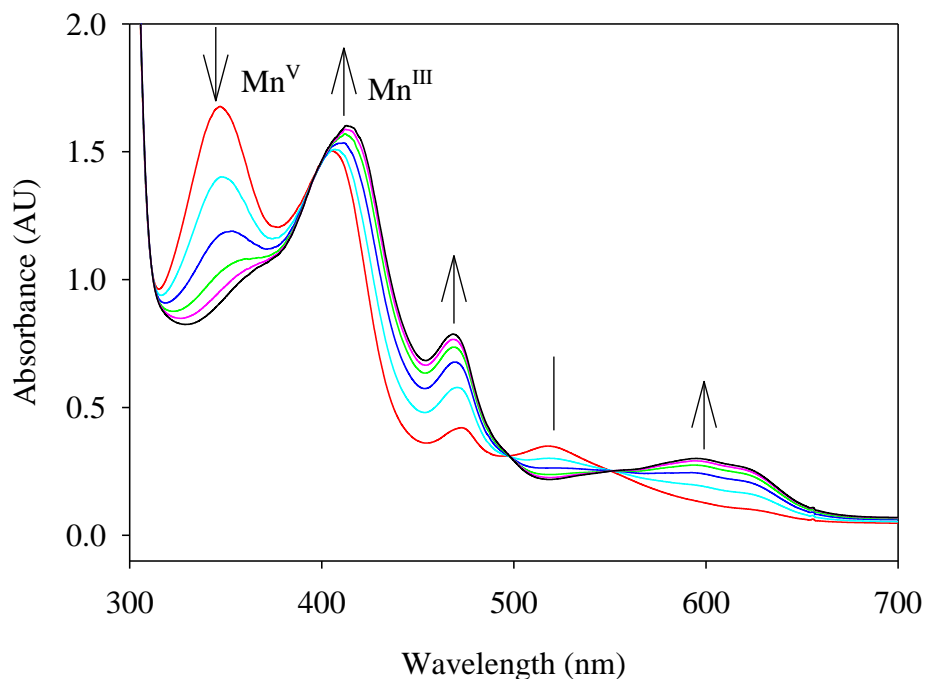


**Figure 21.** Time-resolved UV-vis spectra of the decay of **3a** into **2a** in  $\text{CH}_3\text{CN}$  in the presence or absence of substrate over 3 h.

The solvent effect of **3a** is markedly different from that of metalloporphyrins and other reported metallocorrole systems. Kwong et al. reported that this unique solvent effect is essentially nonexistent with **3b**, which is comparatively not electron deficient, and a manganese(IV) species is formed in all solvents.<sup>35</sup> Figure 23 shows the decay of **4c** into **2c**. Interestingly, **4c** decayed to **2c** consistently in  $\text{CH}_3\text{CN}$ ,  $\text{CH}_2\text{Cl}_2$  and  $\text{CHCl}_3$ .  $\text{CH}_3\text{CN}$  was chosen for further testing of **4c** because of its stability in the solvent.

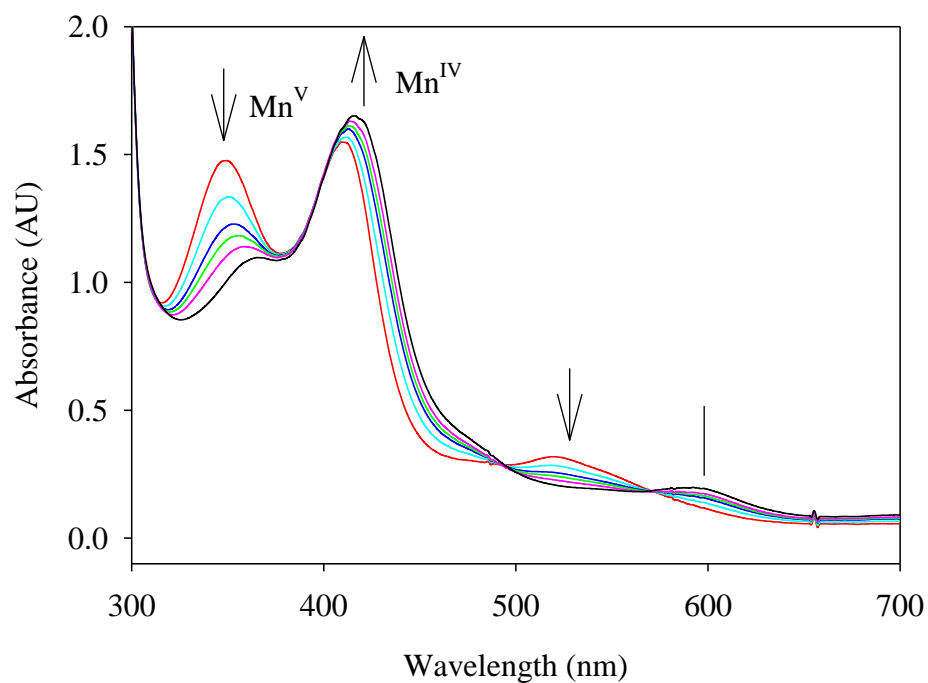


**Figure 22.** Time-resolved spectra of the decay of **3a** in the presence or absence of substrate into a suspected  $\text{Mn}^{\text{IV}}(\text{TPFC})\text{X}$  over 5 h.

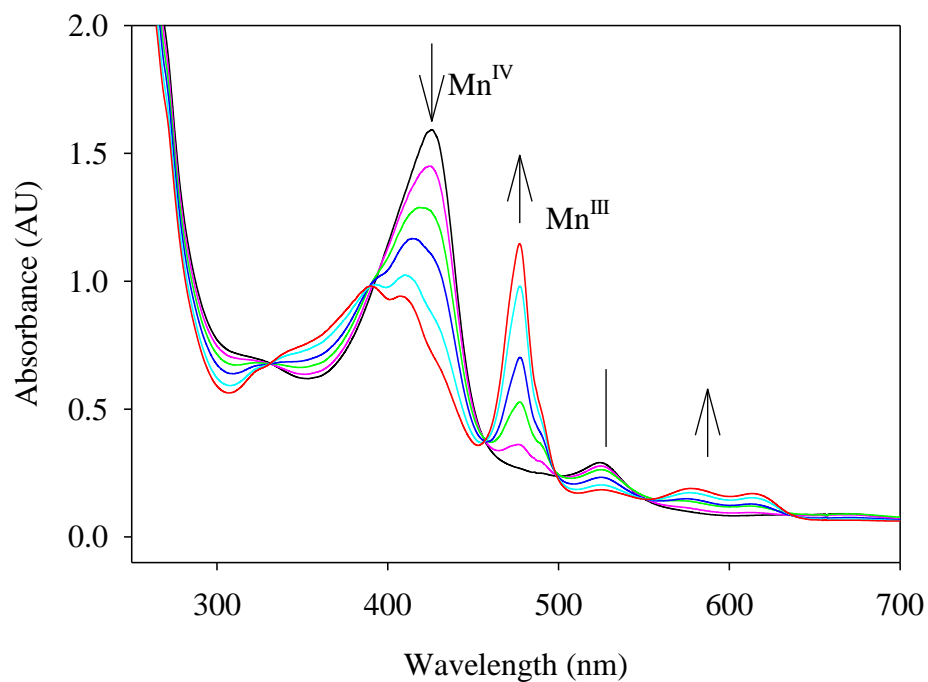


**Figure 23.** Time-resolved spectra of the decay of **4c** into **2c** in  $\text{CH}_3\text{CN}$  in the presence or absence of substrate over 20 min.

### 3.2.3 Kinetic Studies of Oxidations by **3a**

The reactivity of **3a** towards single-turnover OAT to varied substrates was investigated under pseudo-first-order conditions. At minimum, 1000 equiv. of substrate was reacted with a freshly prepared solution of **3a** in the chosen solvent, essentially keeping the concentration of the substrate constant and allowing for an approximated first-order rate constant to be determined from the rate of decay of the 349 nm Soret band. When plotted versus [Sub], the pseudo-first-order rate constants generate a second-order rate constant that more accurately describes the reaction with a particular substrate in a specific solvent. An example kinetic trace and a representative kinetic plot are shown in Figures 24 and 25 for thioanisole. The linearity of the kinetic plot verifies that the concentration of the substrate remains essentially constant, and the  $R^2$  values for these plots range from 0.999–0.983. Table 1 shows second-order rate constants for all substrates in each solvent.

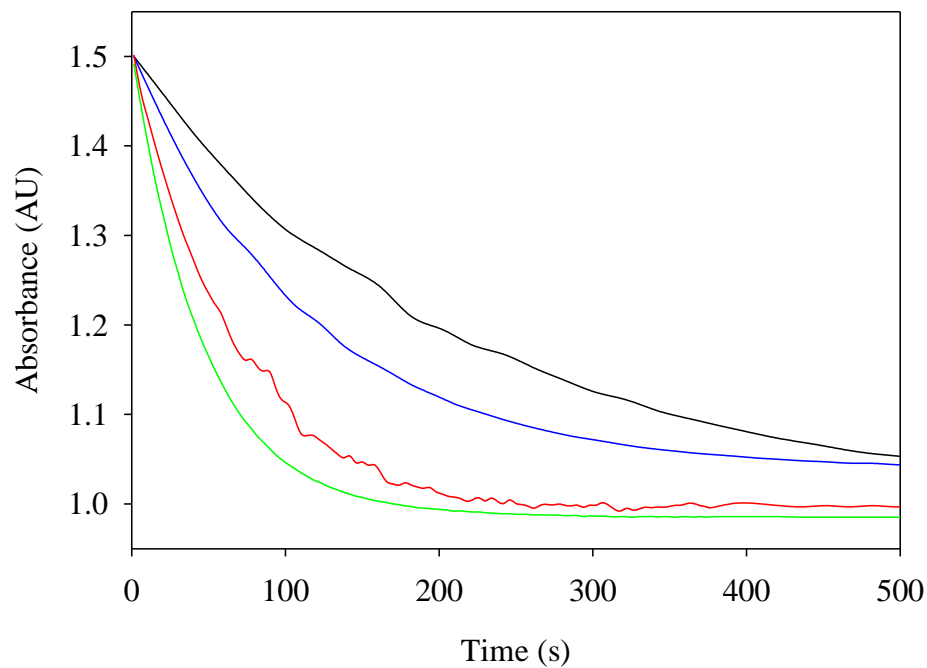


**Figure 24.** Kinetic traces monitored at  $\lambda_{\text{max}} = 349 \text{ nm}$ , showing the decay of **3a** ( $2.5 \times 10^{-5} \text{ M}$ ) into **2a** in  $\text{CH}_2\text{Cl}_2$  with varied concentrations of thioanisole: 10 mM (black), 20 mM (blue), 30 mM (red) and 40 mM (green).

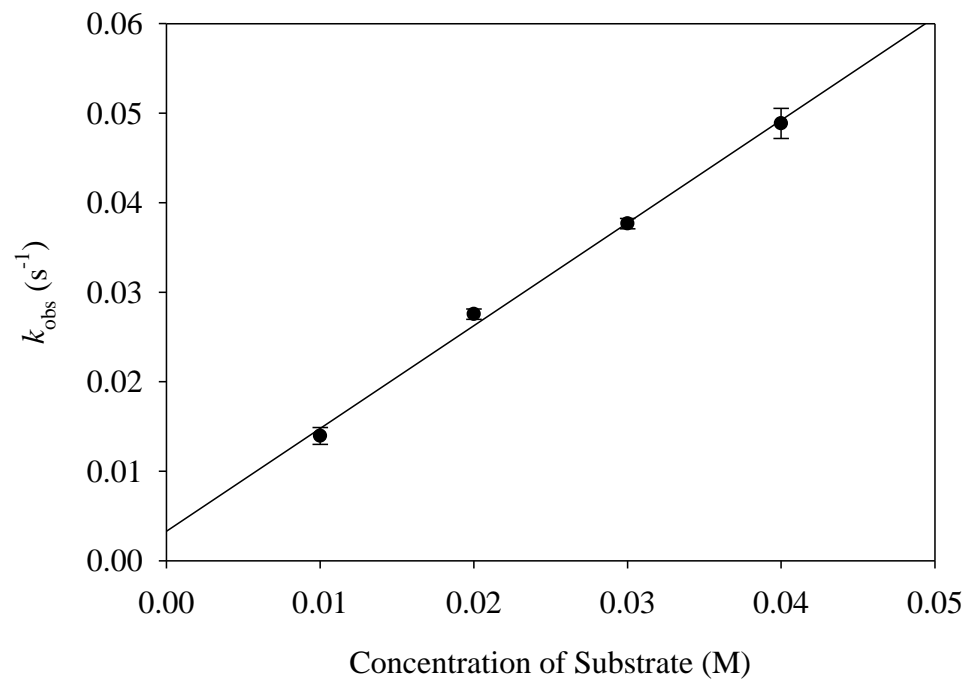


**Figure 25.** A plot of the observed rate constants versus the concentration of thioanisole in  $\text{CH}_3\text{CN}$ . Error bars are reported as  $1\sigma$ .

**Table 1.** Kinetics of oxidation reactions by **3a**<sup>a</sup>

Entry	Substrate	Solvent	$k_2$ ( $\times 10^3$ M <sup>-1</sup> s <sup>-1</sup> )
1	cyclohexene	CH <sub>2</sub> Cl <sub>2</sub>	16 $\pm$ 0.2
2		CH <sub>3</sub> CN	3.9 $\pm$ 0.04
3	<i>cis</i> -cyclooctene	CH <sub>2</sub> Cl <sub>2</sub>	11 $\pm$ 0.8
4		CH <sub>3</sub> CN	2.8 $\pm$ 0.1
5	styrene	CH <sub>2</sub> Cl <sub>2</sub>	3.4 $\pm$ 0.07
6		CH <sub>3</sub> CN	2.4 $\pm$ 0.1
7	ethylbenzene	CH <sub>2</sub> Cl <sub>2</sub>	0.27 $\pm$ 0.03
8	thioanisole	CH <sub>2</sub> Cl <sub>2</sub>	530 $\pm$ 12
9		CH <sub>3</sub> CN	870 $\pm$ 8
10	<i>p</i> -fluorothioanisole	CH <sub>3</sub> CN	1200 $\pm$ 40
11	<i>p</i> -chlorothioanisole	CH <sub>2</sub> Cl <sub>2</sub>	120 $\pm$ 6
12		CH <sub>3</sub> CN	550 $\pm$ 16
13	methyl <i>p</i> -tolyl sulfide	CH <sub>3</sub> CN	2112 $\pm$ 60

<sup>a</sup>In 2.0 mL of solvent with **3a** ( $2.5 \times 10^{-5}$  M) generated *in situ* by oxidation of **2a** with *m*-CPBA (3 equiv.).

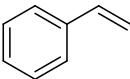
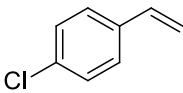
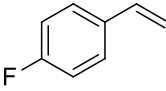
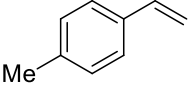
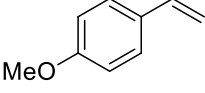
The second-order rate constants for sulfoxidations, epoxidations and hydroxylations follow their relative orders of reactivity, differing by several orders of magnitude. Notably, changing the concentration of **2a** in CH<sub>2</sub>Cl<sub>2</sub> affected the second-order rate constant for the same substrate, clearly indicating that the rate law is not actually first order in **3a**. This effect was not observed in CH<sub>3</sub>CN.



In general, epoxidations are faster in CH<sub>2</sub>Cl<sub>2</sub> than in CH<sub>3</sub>CN, while sulfoxidations follow the opposite pattern. Presumably, sulfoxidations proceed through a different mechanism in which positive charge accumulates on the sulfur.

For comparison, the reactivity of Mn<sup>IV</sup>(TMP)O (**4c**) towards OAT was also studied under single-turnover, pseudo-first-order reaction conditions. In particular, *p*-substituted styrenes were examined. These second-order rate constants are reported in Table 2. **4c** is significantly more reactive towards OAT than **3a** owing to the dianionic nature of the porphyrin ligand. Corrole ligands are trianionic, and consequentially, their high-valent metal complexes are inherently more stable than high-valent metal-oxo porphyrins.

**Table 2.** Rate constants of OAT to *p*-substituted styrenes by **4c**<sup>a</sup>

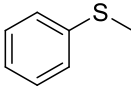
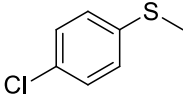
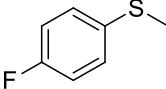
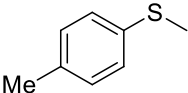
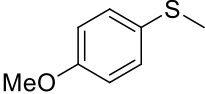
Entry	Substrate	$k_2$ ( $\times 10^3$ M <sup>-1</sup> s <sup>-1</sup> )
1		820 ± 9
2		680 ± 14
3		1100 ± 20
4		1900 ± 50
5		5200 ± 70

<sup>a</sup>In 2.0 mL CH<sub>3</sub>CN with **4c** ( $1.8 \times 10^{-5}$  M) formed *in situ* by oxidation of **2c** by PhI(OAc)<sub>2</sub> (10 equiv.).

### 3.2.4 Hammett Correlation Studies

To more thoroughly probe the OAT mechanism, a series of *p*-substituted thioanisole substrates were oxidized with **3a**. Table 3 shows the second-order rate constants obtained from these substrates. A Hammett plot describes the relationship between the rate constants of reactions with substituted aromatic substrates and a substituent constant  $\sigma^+$ . The substituent constant combines several factors, including electronegativity and electron density, to essentially quantify the electron donating or withdrawing nature of a substituent. Larger values indicate more electron-withdrawing substituents. When the ratio of the rate constants associated with the substituted and unsubstituted substrate is plotted versus  $\sigma^+$ , the resulting linear plot quantifies how significantly the identity of a substituent can affect the rate of a reaction. The slope of the Hammett plot, or reaction constant,  $\rho$ , is specific to the type of reaction. The sign of  $\rho$  indicates whether electron-donating or electron-withdrawing substituents increase the rate of reaction, while the magnitude of  $\rho$  corresponds to the magnitude of the effect. The Hammett plot of substituted thioanisoles with **3a** in CH<sub>3</sub>CN is shown in Figure 26.

**Table 3.** Rate constants of OAT to *p*-substituted thioanisoles by **3a**<sup>a</sup>

Entry	Substrate	$k_2$ ( $\times 10^3 \text{ M}^{-1}\text{s}^{-1}$ )
1		$870 \pm 8$
2		$550 \pm 16$
3		$1200 \pm 40$
4		$2100 \pm 60$
5		$6700 \pm 80$

<sup>a</sup>In 2.0 mL CH<sub>3</sub>CN with **3a** ( $2.5 \times 10^{-5}$  M) formed *in situ* by oxidation of **2a** with *m*-CPBA (3 equiv.).

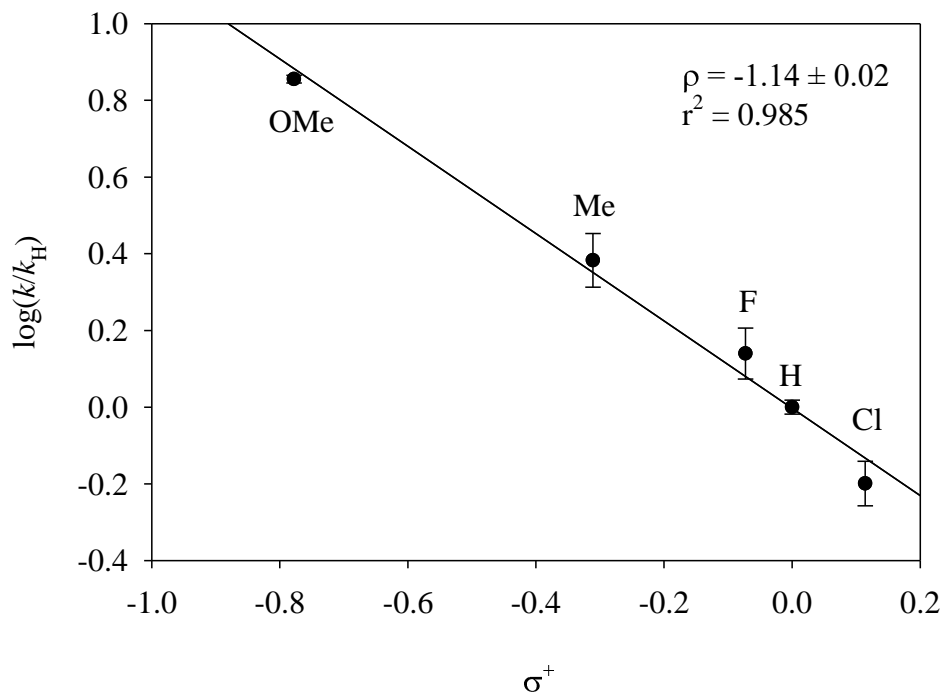


**Figure 26.** The Hammett plot for oxidations of *p*-substituted thioanisoles by **3a** in CH<sub>3</sub>CN.

The slope of  $\rho = -1.14$  is similar to previously-reported values for these reactions under both chemical and photochemical conditions.<sup>35, 53</sup> Given that the slope of  $\rho$  for this plot is negative, the reaction rate is positively affected by electron-donating substituents. This is discernible from Table 3, and it follows the relative reactivities of these substrates towards sulfoxidation. The magnitude of  $\rho$ , however, indicates that the reaction is significantly affected by the nature of the substituents; it describes the selectivity of **3a** as an OAT catalyst. The linearity of the plot implies an electrophilic mechanism, strongly suggesting that the active oxidant in CH<sub>3</sub>CN is **3a**. Notably, the fastest-reacting of these substrates exclusively reformed **2a**, even in CH<sub>2</sub>Cl<sub>2</sub>.

For comparison, a Hammett plot was also constructed from the reactions of **4c** as shown in Table 2. This plot is shown in Figure 27. Although OAT by **4c** is significantly

faster than OAT by **3a**, the effect of the substituents is similar in magnitude and identical in sign; electron donating substituents significantly increase the rate.

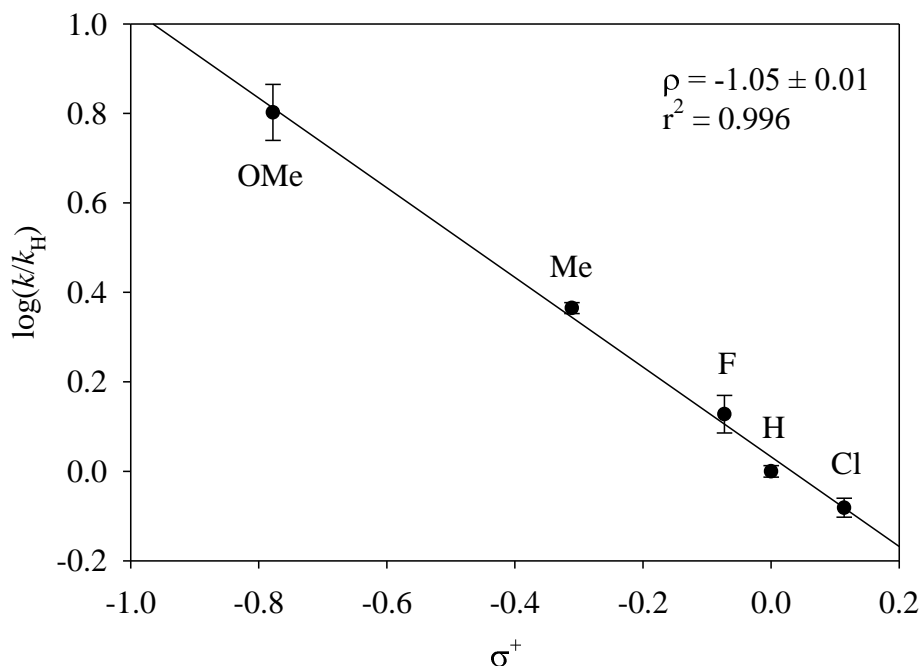
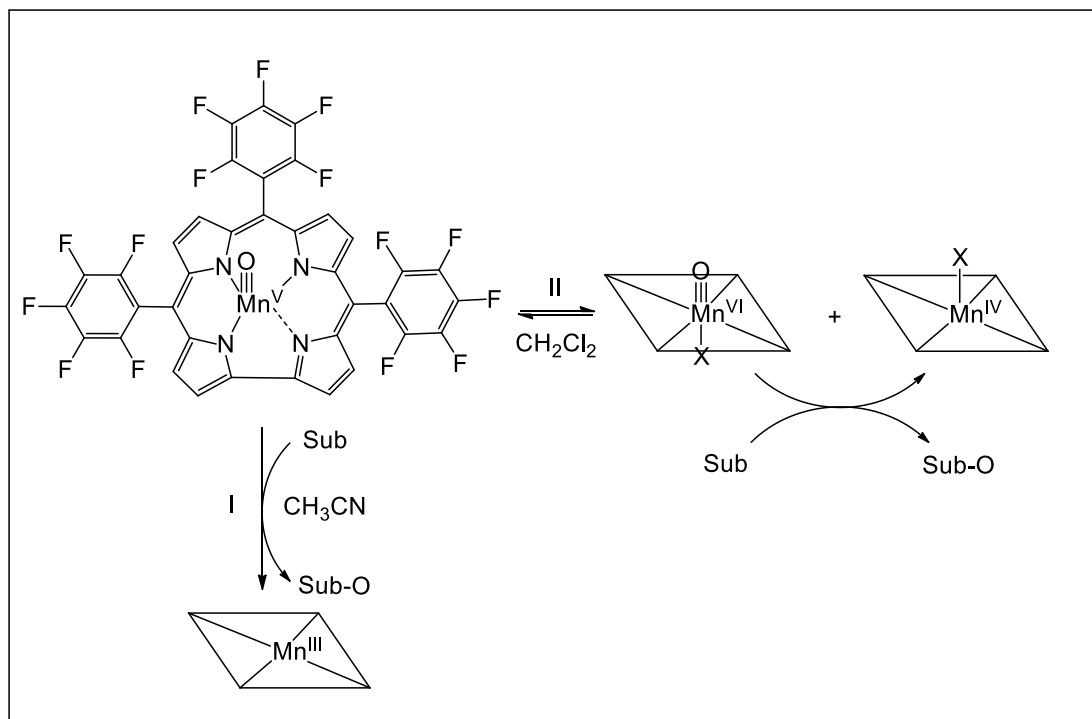


**Figure 27.** The Hammett plot for epoxidations of *p*-substituted styrenes by **4c** in  $\text{CH}_3\text{CN}$ .

### 3.3 Mechanistic Considerations

The significant solvent effect present in this system supports the previously reported two-pathway mechanism of oxidation.<sup>53</sup> This mechanism suggests that the system can either undergo disproportionation or participate in direct oxidation. The disproportionation pathway converts two equivalents of **3a** to one equivalent each of a  $\text{Mn}^{\text{IV}}(\text{TPFC})\text{X}$  and a  $\text{Mn}^{\text{VI}}(\text{TPFC})\text{O}$ , where the manganese(VI) species acts as the active oxidant, and in performing the oxidation, is reduced to the manganese(IV) species. In the direct oxidation pathway, however, **3a** is the active species and directly performs the

oxidation on the substrate, simultaneously being reduced back to **2a**. Both pathways are shown in Scheme 9.



**Scheme 9.** The proposed two-pathway mechanism of oxidation by **3a**. Pathway I is the direct oxidation, while II is the disproportionation pathway.

The products of the decay of **3a** in  $\text{CH}_3\text{CN}$  and  $\text{CH}_2\text{Cl}_2$  support the direct oxidation and disproportionation pathways, respectively; reactions in  $\text{CH}_3\text{CN}$  result in regeneration of **2a**, while reactions in  $\text{CH}_2\text{Cl}_2$  result in accumulation of the manganese(IV) species. Moreover, highly concentrated solutions of **3a** in  $\text{CH}_2\text{Cl}_2$  decomposed faster into the manganese(IV) species than less concentrated solutions. Ideally, the concentration of **3a** should not affect its rate of decay; the effect implies that **3a** disproportionates, contributing to the accumulation of the manganese(IV) species. Essentially, the rate law is not first order in **3a**. This further supports the suggestion of a disproportionation pathway; Newcomb et al. proved using the steady-state

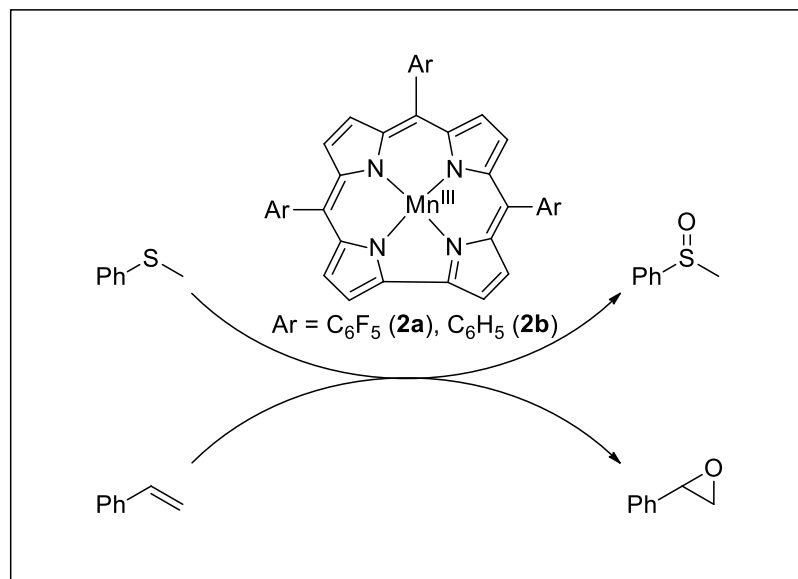
approximation that disproportionation would result in a fractional order for **3a**.<sup>65</sup> This multiple-pathway mechanism is also supported by the report of a similar solvent effect under photochemical conditions. Kwong et al. reported a two-pathway, solvent-dependent mechanism of oxidation by photochemically-generated **3a**.<sup>35</sup>

## 4. CATALYTIC OXIDATIONS BY MANGANESE CORROLES

### 4.1 Introduction

Iodobenzene diacetate [ $\text{PhI}(\text{OAc})_2$ ] was chosen as the sacrificial oxidant for catalytic oxidations (Scheme 10).  $\text{PhI}(\text{OAc})_2$  is milder than commonly used oxidants such as *m*-CPBA, *tert*-butyl-hydroperoxide (TBHP) or iodosylbenzene (PhIO), each of which can bleach the catalyst, resulting in low catalytic efficiency. Additionally, these strong oxidants can directly oxidize the substrates, artificially increasing yields of oxidized products. Particularly, *m*-CPBA performs nearly quantitative epoxidation of alkenes. Under single-turnover, pseudo-first-order conditions, as outlined in the previous kinetic studies, the use of *m*-CPBA is not a concern because of the comparatively high concentrations of substrate. However, under catalytic conditions, the amount of sacrificial oxidant needed to propagate the catalytic cycle is significantly larger; in turn, the use of an oxidant that reacts with the substrate becomes less feasible.  $\text{PhI}(\text{OAc})_2$  is commercially available, and it is significantly safer to handle than stronger oxidants. In this section, the utility of  $\text{PhI}(\text{OAc})_2$  was further explored for the catalytic oxidation of alkenes and sulfides by manganese corrole complexes.





**Scheme 10.** Catalytic sulfoxidations and epoxidations by manganese(III) corroles.

## 4.2 Screening Studies

### 4.2.1 Solvent Effect

In an effort to determine optimal conditions for catalysis, screening studies were first performed. Given that a significant solvent effect on the OAT mechanism has been established in the previous section, the solvent effect was reexamined under catalytic conditions. The epoxidation of *cis*-cyclooctene was chosen as the probe for screening studies because of the relatively clean product, typically resulting in the epoxide only. Allylic oxidation to the corresponding alcohol or over-oxidation to the ketone often interferes with the epoxidation of cyclohexene. Likewise, sulfides can be overoxidized to form sulfones as opposed to the desirable sulfoxides. Table 4 shows the conversion of *cis*-cyclooctene to *cis*-cyclooctene oxide in  $\text{CH}_2\text{Cl}_2$ ,  $\text{CH}_3\text{CN}$  and  $\text{CH}_3\text{OH}$  by **2a**.

**Table 4.** Solvent effect on the epoxidation of *cis*-cyclooctene by **2a**<sup>a</sup>

Entry	Solvent	Time (h)	Conversion (%) <sup>c</sup>
1	dichloromethane	3	10
2		5	11
3	methanol	3	10
4		5	13
5 <sup>b</sup>		3	28
6	acetonitrile	3	11
7		5	13
8 <sup>b</sup>		3	33

<sup>a</sup>Unless otherwise noted, all reactions took place in 0.5 mL of solvent at 23 ± 2 °C with 0.2 mol% of **2a**, 0.2 mmol *cis*-cyclooctene and 0.3 mmol PhI(OAc)<sub>2</sub>.

<sup>b</sup>40 ± 2 °C.

<sup>c</sup>Determined by GC-MS analysis of the crude reaction mixture.

The reaction in dichloromethane was examined at 3 h, and *cis*-cyclooctene oxide was obtained as the only identifiable product at ca. 10% conversion (Table 4, entry 1). Slightly higher conversions were obtained after 5 h of reaction (entry 2). The slowing of the reaction over the course of the last 2 h indicates that the catalyst was bleached during the catalytic cycle. This is supported by observations of the color change of the solutions; the bright red color of the dichloromethane and acetonitrile solutions began to fade after about 3 h of reaction. Highest conversions at room temperature were seen in acetonitrile, while dichloromethane exhibited the lowest conversions (entry 2, entry 7).

All reactions benefitted from higher reaction temperature, and conversions of up to 33% were reached when heated to 40 °C (entry 8).

Notably, **2a** is catalytically active in methanol, resulting in conversions of 28% with heating (entry 5). However, **3a** was unable to be formed during the single-turnover kinetic studies. Methanol, which can form hydrogen bonds, may strongly coordinate to the metal, potentially preventing the binding of an oxygen source, which is crucial for the formation of a high-valent metal-oxo species. However, this is unlikely given the significant catalytic activity in this solvent; a high-valent metal-oxo species is proposed as the major oxidizing intermediate in the catalytic cycles of metallocorrole- and metalloporphyrin-catalyzed oxidations. Alternatively, the high-valent metal-oxo species could be so reactive in this solvent that it is reacted faster than it is formed, preventing the detection of this intermediate. The latter explanation is more reasonable because it accounts for the considerable catalytic activity in the solvent. Because CH<sub>3</sub>CN exhibited the highest conversions, it was chosen for all remaining catalytic reactions with **2a**. For comparison, the solvent effect on the catalytic epoxidation of *cis*-cyclooctene by **2b** was also examined. Similar results were obtained and are shown in Table 5.

**Table 5.** Solvent effect on the epoxidation of *cis*-cyclooctene by **2b**<sup>a</sup>

Entry	Solvent	Time (h)	Conversion (%) <sup>c</sup>
1	dichloromethane	3	6
2		5	8
3	methanol	3	7
4		5	10
5 <sup>b</sup>		3	18
6	acetonitrile	3	7
7		5	11
8 <sup>b</sup>		3	22

<sup>a</sup>Unless otherwise noted, all reactions took place in 0.5 mL of solvent at 23 ± 2 °C with 0.2 mol% **2b**, 0.2 mmol *cis*-cyclooctene and 0.3 mmol PhI(OAc)<sub>2</sub>.

<sup>b</sup>40 ± 2 °C

<sup>c</sup>Determined by GC-MS analysis of the crude reaction mixture.

The general trends in reactivity are similar to those of **2a**. The reaction in dichloromethane was examined at 3 h, and *cis*-cyclooctene oxide was obtained as the only identifiable product with ca. 6% conversion (Table 5, entry 1). As with **2a**, the reaction slowed over the course of the last 2 h, giving only an 8% conversion after 5 h total reaction time (entry 2), indicating catalyst bleaching. All reactions benefitted from heating, and in acetonitrile, conversions of 22% were reached with heating (entry 8). Acetonitrile shows the highest conversions of about 11% with no heating (entry 7) compared to dichloromethane's 8% under the same conditions (entry 2). Again, there

was catalytic activity in methanol, and ca. 10% conversion was obtained at room temperature (entry 4).

Interestingly, **2b** yielded lower conversions in all solvents. This is likely related to the electron-deficient nature of the pentafluorophenyl groups on **2a**, resulting in a more reactive high-valent manganese(V)-oxo species in comparison to **2b**. Additionally, fluorination of the corrole ligand in **2a** can increase its stability against catalyst bleaching under catalytic conditions.

#### 4.2.2 Water Effect

In several metalloporphyrins and a reported iron(III) corrole with  $\text{PhI}(\text{OAc})_2$ , catalytic efficiency is increased with the addition of small amounts of water. According to Chen et al., this effect is likely due to the hydrolysis of  $\text{PhI}(\text{OAc})_2$  into the stronger oxidant  $\text{PhIO}$ .<sup>66</sup> This explanation is also supported by the decrease in selectivity of the reported iron(III) corrole catalyst upon addition of water. Interestingly, catalytic activity for the reported iron(III) corrole and for reported metalloporphyrins began to decrease upon larger addition of water. In essence, these catalysts exhibited maximum conversions with small amounts of added water, and the conversion subsequently decreased as more water was added. This effect is most likely due to the highly polar nature of water; it can coordinate with the metal center and prevent the formation of critical high-valent metal-oxo species. The epoxidation of *cis*-cyclooctene by **2a** with added water was examined, and the results are present in Table 6.

**Table 6.** Water effect on the epoxidation of *cis*-cyclooctene by **2a**<sup>a</sup>

Entry	Water ( $\mu\text{L}$ )	Conversion (%) <sup>b</sup>
1	0	18
2	5	16
3	10	15
4	20	14
5	40	11

<sup>a</sup>All reactions took place in 0.5 mL CH<sub>3</sub>CN at 23  $\pm$  2 °C with 0.2 mol% **2a**, 0.2 mmol *cis*-cyclooctene and 0.3 mmol PhI(OAc)<sub>2</sub> over 24 h.

<sup>b</sup>Determined by GC-MS analysis of the crude reaction mixture.

Of note, **2a** expresses no positive water effect. Even the miniscule addition of 5  $\mu\text{L}$  negatively affects conversions (Table 6, entry 2). This may indicate that water coordinates more strongly to manganese(III) corroles than to iron(III) corroles, possibly reducing the formation rate of the high-valent manganese-oxo intermediate. For comparison, the epoxidation of *cis*-cyclooctene by **2b** was also tested under these conditions, and results are present in Table 7.

**Table 7.** Water effect on the epoxidation of *cis*-cyclooctene by **2b**<sup>a</sup>

Entry	Water ( $\mu\text{L}$ )	Conversion (%)
1	0	14
2	5	12
3	10	11
4	20	9
5	40	6

<sup>a</sup>All reactions took place in 0.5 mL CH<sub>3</sub>CN at 23  $\pm$  2 °C with 0.2 mol% **2b**, 0.2 mmol *cis*-cyclooctene and 0.3 mmol PhI(OAc)<sub>2</sub> over 24 h.

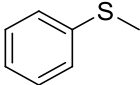
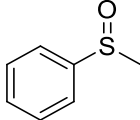
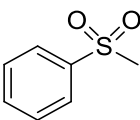
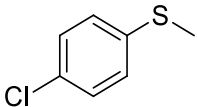
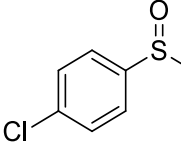
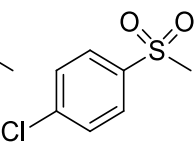
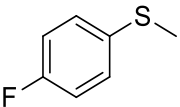
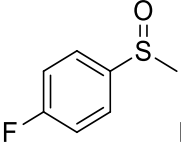
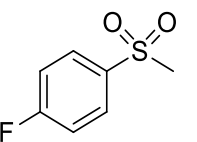
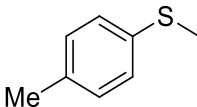
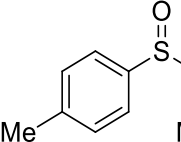
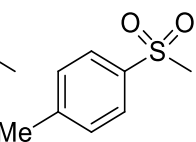
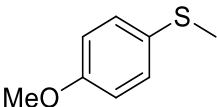
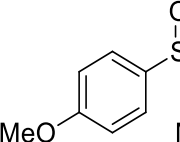
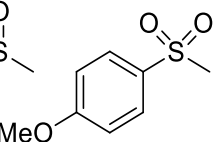
<sup>b</sup>Determined by GC-MS analysis of the crude reaction mixture.

**2b** exhibits essentially the same water effect as **2a**, indicating that the lack of a positive water effect is likely unrelated to the corrole ligand itself, and instead more relevant to the manganese(III) center. This supports the assertion that the unique water effect is caused by strong coordination between the manganese center and water, preventing the formation of the manganese(V)-oxo species and thus slowing down the catalytic cycle.

#### 4.3 Catalytic Oxidations of Sulfides to Sulfoxides

Catalytic sulfoxidations by **2a** were investigated based on the results of the screening studies. Table 8 shows the results of sulfoxidations of *p*-substituted thioanisoles.

**Table 8.** Catalytic sulfoxidation of *p*-substituted thioanisoles by **2a**<sup>a</sup>

Entry	Substrate	Products	Conversion	Product
			(%) <sup>b</sup>	Ratio <sup>c</sup>
1		 	49	67:33
2		 	53	62:38
3		 	47	57:43
4		 	57	54:46
5		 	59	51:49

<sup>a</sup>All reactions took place in 0.5 mL CH<sub>3</sub>CN at 23 ± 2 °C with 0.2 mol% **2b**, 0.2 mmol substrate and 0.3 mmol PhI(OAc)<sub>2</sub> over 5 h.

<sup>b</sup>Determined by GC-MS analysis of the crude reaction mixture.

<sup>c</sup>Ratio of sulfoxide:sulfone products.

The sulfoxidation of thioanisole resulted in only 49% conversion with 2:1 formation of the sulfoxide over the sulfone (Table 8, entry 1). The incomplete conversion of substrate is due to catalyst bleaching. As expected based on the Hammett correlation studies, catalytic conversions increased with more electron-rich substrates.

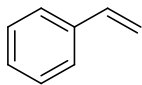
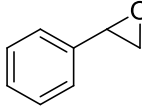
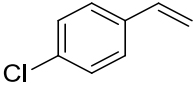
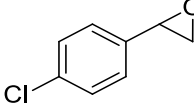
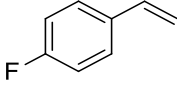
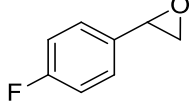
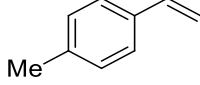
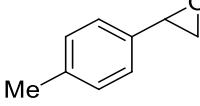
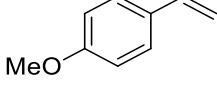
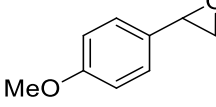


The *p*-methoxythioanisole had conversions of 59% (entry 5), while selectivity dropped to a nearly even mix of the two products.

#### 4.4 Catalytic Epoxidation of Alkenes

Catalytic epoxidations of *p*-substituted styrenes by **2a** were investigated under the optimal conditions from the screening studies. These data are shown in Table 9.

**Table 9.** Catalytic epoxidation of *p*-substituted styrenes by **2a**<sup>a</sup>

Entry	Substrate	Product	Conversion (%) <sup>b</sup>	Product Ratio <sup>c</sup>
1			28	68:11:21
2			29	57:11:32
3			31	54:11:35
4			36	52:17:31
5			39	52:48 <sup>d</sup>

<sup>a</sup>All reactions took place in 0.5 mL CH<sub>3</sub>CN at 23 ± 2 °C with 0.2 mol% **2b**, 0.2 mmol substrate and 0.3 mmol PhI(OAc)<sub>2</sub> over 5 h.

<sup>b</sup>Determined by GC-MS analysis of the crude reaction mixtures.

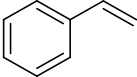
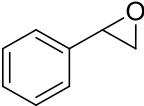
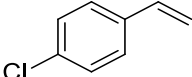
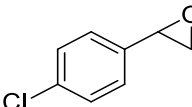
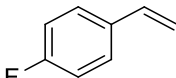
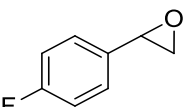
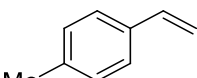
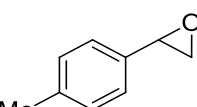
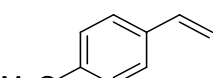
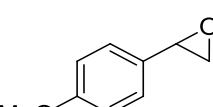
<sup>c</sup>Ratio of epoxide:benzaldehyde:phenylacetaldehyde products

<sup>d</sup>Ratio of epoxide:benzyl alcohol products

The oxidation of styrene over 5 h yielded a mixture of products, including the epoxide, benzaldehyde and phenylacetaldehyde with 68% selectivity of epoxide formation (Table 9, entry 1). As with sulfoxidation, there is a clear trend wherein electron-donating *p*-substituents increase the conversions, and the *p*-fluorostyrene substrate resulted in higher conversions than the unsubstituted styrene at 31 and 28%, respectively (entry 1, entry 3). Selectivity decreased as reactivity increased, with the most reactive *p*-methoxystyrene reaching conversions of 39%, but yielding only 52% epoxide product. For comparison, **2c** was used to perform the same epoxidations under similar conditions established for manganese porphyrin catalysis.<sup>18</sup> Results are shown in Table 10.

After 5 h of reaction in literature-established conditions for manganese porphyrin catalysis, near quantitative conversion was reached for even the unsubstituted styrene (Table 10, entry 1). The selectivity, however, is diminished to only 55% epoxide. The selectivity decreases with more electron-donating substituents, where the *p*-fluorostyrene substrate resulted in only 49% epoxide and significant amounts of the benzaldehyde and phenylacetaldehyde overoxidized products (entry 3). Additionally, the most reactive *p*-methoxystyrene produced three distinct overoxidized products in addition to the desired epoxide, including a 1° and 2° benzyl alcohol and a ketone. Although the metalloporphyrin catalyst was more reactive, giving near quantitative conversions, the selectivity is diminished compared to the less reactive metallocorrole catalyst.

**Table 10.** Catalytic epoxidation of *p*-substituted styrenes by **2c**<sup>a</sup>

Entry	Substrate	Products	Conversion (%) <sup>b</sup>	Product Ratio <sup>c</sup>
1			99	55:12:33
2			99	51:17:32
3			100	49:16:35
4			100	48:17:35
5			100	44:12:10:33 <sup>d</sup>

<sup>a</sup>All reactions took place in 0.5 mL CH<sub>3</sub>CN at 23 ± 2 °C with 0.2 mol% **2c**, 0.2 mmol substrate, 5 μL H<sub>2</sub>O and 0.3 mmol PhI(OAc)<sub>2</sub> over 5 h.

<sup>b</sup>Determined by GC-MS analysis of the crude reaction mixture.

<sup>c</sup>Ratio of epoxide:benzaldehyde:phenylacetaldehyde products

<sup>d</sup>Ratio of epoxide:1° benzyl alcohol:ketone:2° benzyl alcohol products

## 5. CONCLUSIONS

In this work, manganese porphyrin and corrole systems (**2**) were synthesized as biomimetic models of Cytochrome P450 enzymes and subsequently characterized by UV-vis absorbance and  $^1\text{H-NMR}$ . The role of high-valent manganese-oxo species in OAT by these systems was examined, and the catalytic abilities of these complexes towards epoxidation and sulfoxidation with  $\text{PhI}(\text{OAc})_2$  as an oxygen source were explored.

Manganese(V)-oxo corroles (**3**) and a manganese(IV)-oxo porphyrin (**4**) were generated from oxidation of the corresponding manganese(III) precursors (**2**) using *m*-chloroperoxybenzoic acid (*m*-CPBA) as an oxygen source. Under single-turnover conditions, **3** complexes showed appreciable reactivity towards sulfoxidation, epoxidation and hydroxylation. In the tris(pentafluorophenyl)corrole system (**3a**), results from spectral studies indicate that the active oxidizing intermediate is solvent-dependent. In acetonitrile, the active oxidizing intermediate is most likely the manganese(V)-oxo species (**3a**). However, in dichloromethane, the active oxidant is suspected to be a putative manganese(VI)-oxo species generated from disproportionation of the manganese(V)-oxo species. This significant solvent effect is not present in other reported manganese corrole or porphyrin systems.

The catalytic activity of tris(pentafluorophenyl)corrolato manganese(III) (**2a**) towards thioanisoles and styrenes was examined with iodobenzene diacetate [ $\text{PhI}(\text{OAc})_2$ ] as a mild oxygen source. This complex was then compared to triphenylcorrolato manganese(III) (**2b**) and tetramesitylporphyrinato manganese(III) (**2c**). **2a** exhibited higher conversions than **2b**, most likely because of the relative

stability of **3b** compared to **3a**. In contrast, **2c** was much more reactive than **2a**, resulting in much higher conversions, but much less selectivity. Previously reported manganese porphyrin and iron corrole systems showed an accelerating effect upon addition of small amounts of water, attributed to the hydrolysis of the oxygen source to the more reactive iodosylbenzene (PhIO). In contrast to these systems, **2a** and **2b** did not have a positive water effect, but instead had decreased conversions with any added water. This is attributed to the strong coordination between manganese(III) and water, preventing the oxygen source from coordinating with the metal center. This coordination is crucial to generate the active metal-oxo intermediate.

The use of metallocorrole catalysts for selective oxidations is widely applicable. Most notably, selective sulfoxidation is relevant in the synthesis of many pharmaceuticals, including proton pump inhibitors. In the literature, **3a** has been generated under photochemical conditions and used to perform OAT under environmentally-friendly conditions.<sup>35</sup> Currently, our lab is exploring the photochemical generation of other high-valent metallocorroles and metalloporphyrins for environmentally-friendly oxidations.

## REFERENCES

1. Sheldon, R. A., *Metalloporphyrins in Catalytic Oxidations*. Marcel Dekker: New York, 1994.
2. Ortiz de Montellano, P. R., *Cytochrome P450 Structure, Mechanism, and Biochemistry*. 3rd ed.; Kluwer Academic/Plenum: New York, 2005.
3. Brink, G. T., Green, Catalytic Oxidation of Alcohols in Water. *Science* **2000**, 287 (5458), 1636-1639.
4. Punniyamurthy, T.; Velusamy, S.; Iqbal, J., Recent Advances in Transition Metal Catalyzed Oxidation of Organic Substrates with Molecular Oxygen. *Chem.Rev.* **2005**, 105 (6), 2329-2363.
5. Poulos, T. L.; Finzel, B. C.; Howard, A. J., Crystal Structure of Substrate-Free *Pseudomonas putida* Cytochrome P450. *Biochemistry* **1986**, 25, 5314-5322.
6. Nelson, D. R.; Kamataki, T.; Waxman, D. J.; Guengerich, F. P.; Estabrook, R. W.; Feyereisen, R.; Gonzalez, F. J.; Coon, M. J.; Gunsalus, I. C.; Gotoh, O., The P450 Superfamily: Update on New Sequences, Gene Mapping, Accession Numbers, Early Trivial Names of Enzymes, and Nomenclature. *DNA Cell Biol.* **1993**, 12 (1), 1-51.
7. Wrighton, S. A.; Stevens, J. C., The Human Hepatic Cytochromes P450 Involved in Drug Metabolism. *Crit. Rev. Toxicol.* **1992**, 22 (1), 1-21.
8. Hasemann, C. A.; Kurumbail, R. G.; Boddupalli, S. S.; Peterson, J. A.; Deisenhofer, J., Structure and Function of Cytochromes P450: A Comparative Analysis of Three Crystal Structures. *Structure* **1995**, 3 (1), 41-62.
9. Sono, M.; Roach, M. P.; Coulter, E. D.; Dawson, J. H., Heme-Containing Oxygenases. *Chem. Rev.* **1996**, 96 (7), 2841-2887.

10. Denisov, I. G.; Makris, T. M.; Sligar, S. G.; Schlichting, I., Structure and chemistry of cytochrome P 450. *Chem. Rev.* **2005**, *105* (6), 2253-2277.
11. Poulos, T. L.; Finzel, B. C.; Howard, A. J., High-resolution Crystal Structure of Cytochrome P450<sub>cam</sub>. *J. Mol. Biol.* **1987**, *195*, 687-700.
12. Marques, S.; Ramos, J. L., Transcriptional Control of the *Pseudomonas putida* TOL plasmid catabolic pathways. *Mol. Microbiol.* **1993**, *9* (5), 923-929.
13. Meunier, B., *Metal-Oxo and Metal-Peroxo Species in Catalytic Oxidations*. Springer-Verlag: Berlin, 2000.
14. Meunier, B.; Visser, S. I.; Shaik, S., Mechanism of Oxidation Reactions Catalyzed by Cytochrome P450 Enzymes. *Chem. Rev.* **2004**, *104*, 3947-3980.
15. Che, C.-M.; Huang, J.-S., Metalloporphyrin-based oxidation systems: from bioimetic reactions to application in organic synthesis. *Chem. Commun.* **2009**, 3996-4015.
16. Meunier, B., Metalloporphyrins as Versatile Catalysts for Oxidation Reactions and Oxidative DNA Cleavage. *Chem. Rev.* **1992**, *92* (6), 1411-1456.
17. Rittle, J.; Green, M. T., Cytochrome P450 Compound I: Capture, Characterization, and C-H Bond Activation Kinetics. *Science* **2010**, *330*, 933-937.
18. Kwong, K. W.; Chen, T. H.; Luo, W.; Jeddi, H.; Zhang, R., A biomimetic oxidation catalyzed by manganese(III) porphyrins and iodobenzene diacetate: Synthetic and mechanistic investigations. *Inorg. Chim. Acta* **2015**, *430*, 176-183.
19. Nam, W., High-Valent Iron(IV)-Oxo Complexes of Heme and Non-Heme Ligands in Oxygenation Reactions. *Acc. Chem. Res.* **2007**, *40*, 522-531.

20. Che, C.-M.; Yu, W.-Y., Ruthenium-oxo and -tosylimido porphyrin complexes for epoxidation and aziridination of alkenes. *Pure and Applied Chemistry* **1999**, *71* (2), 281-288.
21. Gross, Z.; Ini, S., Asymmetric Catalysis by a Chiral Ruthenium Porphyrin: Epoxidation, Hydroxylation, and Partial Kinetic Resolution of Hydrocarbons. *Org. Lett.* **1999**, *1* (13), 2077-2080.
22. Groves, J. T., Reactivity and Mechanisms of Metalloporphyrin-Catalyzed Oxidations. *J. Porph. Phthal.* **2000**, *4*, 350-352.
23. Groves, J. T.; Haushalter, R. C.; Nakamura, M.; Nemo, T. E.; Evans, B. J., High-valent iron-porphyrin complexes related to peroxidase and cytochrome P-450. *J. Am. Chem. Soc.* **1981**, *103* (10), 2884-6.
24. Groves, J. T. K., William J., Jr.; Haushalter, Robert C., Hydrocarbon oxidations with oxometalloporphyrins. Isolation and reactions of a (porphyrinato)manganese(V) complex. *J. Am. Chem. Soc.* **1980**, *102* (20), 6375-7.
25. Groves, J. T.; Stern, M. K., Olefin epoxidation by manganese (IV) porphyrins: evidence for two reaction pathways. *J. Am. Chem. Soc.* **1987**, *109* (12), 3812-14.
26. Leeladee, P.; Goldberg, D. P., Epoxidations Catalyzed by Manganese(V) Oxo and Imido Complexes: Role of the Oxidant-Mn-Oxo (Imido) Intermediate. *Inorg. Chem.* **2010**, *49*, 3083-3085.
27. Bougher, C. J.; Liu, S.; Hicks, S. D.; Abu-Omar, M. M., Valence Tautomerization of High-Valent Manganese(V)-Oxo Corrole Induced by Protonation of the Oxo Ligand. *J. Am. Chem. Soc.* **2015**, *137*, 14481-14487.



28. Leeladee, P.; Baglia, R. A.; Prokop, K. A.; Latifi, R.; de Visser, S. P.; Goldberg, D. P., Valence Tautomerism in a High-Valent Manganese-Oxo Porphyrinoid Complex Induced by a Lewis Acid. *J. Am. Chem. Soc.* **2012**, *134* (25), 10397-10400.
29. Zaragoza, J. P.; Baglia, R. A.; Siegler, M. A.; Goldberg, D. P., Strong Inhibition of O-Atom Transfer Reactivity for Mn<sup>IV</sup>(O)(pi-Radical-Cation)(Lewis Acid) versus Mn<sup>V</sup>(O) Porphyrinoid Complexes. *J. Am. Chem. Soc.* **2015**, *137* (20), 6531-6540.
30. Baglia, R. A.; Prokop-Prigge, K. A.; Neu, H. M.; Siegler, M. A.; Goldberg, D. P., Mn(V)(O) versus Cr(V)(O) Porphyrinoid Complexes: Structural Characterization and Implications for Basicity Controlling H-Atom Abstraction. *J. Am. Chem. Soc.* **2015**, *137* (34), 10874-10877.
31. Groves, J. T.; Nemo, T. E.; Myers, R. S., Hydroxylation and Epoxidation Catalyzed by Iron-Porphine Complexes. Oxygen Transfer from Iodosylbenzene. *J. Am. Chem. Soc.* **1979**, *101*, 1032-1033.
32. Nam, W.; Kim, I.; Lim, M. H.; Choi, H. J.; Lee, J. S.; Jang, H. G., Isolation of an oxomanganese(V) porphyrin intermediate in the reaction of a manganese(III) porphyrin complex and H<sub>2</sub>O<sub>2</sub> in aqueous solution. *Chem. Eur. J.* **2002**, *8* (9), 2067-2071.
33. Collman, J. P.; Chien, A. S.; Eberspacher, T. A.; Brauman, J. I., Multiple Active Oxidants in Cytochrome P-450 Model Oxidations. *J. Am. Chem. Soc.* **2000**, *122* (45), 11098-11100.
34. In, J. H.; Park, S. E.; Song, R.; Nam, W., Iodobenzene diacetate as an efficient terminal oxidant in iron(III) porphyrin complex-catalyzed oxygenation reactions. *Inorg. Chim. Acta* **2003**, *343*, 373-376.

35. Kwong, K. W.; Lee, N. F.; Ranburger, D.; Malone, J.; Zhang, R., Visible Light-Induced Formation of Corrole-Manganese(V)-Oxo Complexes: Observation of Multiple Oxidation Pathways. *J. Inorg. Biochem.* **2016**, *163*, 39-44.
36. Suslick, K. S.; Watson, R. A., The photochemistry of chromium, manganese, and iron porphyrin complexes. *New J. Chem.* **1992**, *16* (5), 633-42.
37. Hoshino, M. A., S.; Yamaji, M.; Hama, Y., Laser photolysis studies of nitric oxide adducts of cobalt(II) porphyrins. Photoinduced denitrosylation at the temperature range 160-300 K. *J. Phys. Chem.* **1986**, *90*, 2109-2111.
38. Groves, J. T.; Quinn, R., Aerobic epoxidation of olefins with ruthenium porphyrin catalysts. *J. Am. Chem. Soc.* **1985**, *107* (20), 5790-2.
39. Hodgkin, D. C.; Pickworth, J.; Robertson, J. H.; Trueblood, K. N.; Prosen, R. J.; White, J. G., Structure of Vitamin B<sub>12</sub>: The Crystal Structure of the Hexacarboxylic Acid Derived from B<sub>12</sub> and the Molecular Structure of the Vitamin. *Nature* **1955**, *176* (325-328).
40. Visser, S. P.; Ogliaro, F.; Gross, Z.; Shaik, S., What is the Difference between the Manganese Porphyrin and Corrole Analogues of Cytochrome P450's Compound I? *Chem. Eur. J.* **2001**, *7*, 4954-4960.
41. Johnson, A. W.; Kay, I. T., Corroles. Part I. Synthesis. *J. Chem. Soc.* **1965**, *306*, 1620-1629.
42. Gross, Z.; Galili, N.; Simkhovich, L.; Saltsman, I.; Botoshansky, M.; Blaeser, D.; Boese, R.; Goldberg, I., Solvent-Free Condensation of Pyrrole and Pentafluorobenzaldehyde: A Novel Synthetic Pathway to Corrole and Oligopyrromethenes. *Org. Lett.* **1999**, *1* (4), 599-602.

43. Agadjanian, H.; Weaver, J. J.; Mahammed, A.; Rentsendorj, A.; Bass, S.; Kim, J.; Dmochowski, I. J.; Margalit, R.; Gray, H. B.; Gross, Z.; Medina-Kauwe, L. K., Specific Delivery of Corroles to Cells via Noncovalent Conjugates with Viral Proteins. *Pharm. Res.* **2006**, *23*, 367-377.
44. Agadjanian, H.; Ma, J.; Rentsendorj, A.; Valluripalli, V.; Hwang, J. Y.; Mahammed, A.; Farkas, D. L.; Gray, H. B.; Gross, Z.; Medina-Kauwe, L. K., Tumor Detection and Elimination by a Targeted Gallium Corrole. *Proc. Natl. Acad. Sci. U.S.A.* **2009**, *106* (15), 6105-6110.
45. Teo, R. D.; Gray, H. B.; Lim, P.; Termini, J.; Domeshek, E.; Gross, Z., A Cytotoxic and Cytostatic Gold(III) Corrole. *Chem. Commun.* **2014**, *50*, 13789-13792.
46. Hwang, J. Y.; Lubow, J.; Chu, D.; Ma, J.; Agadjanian, H.; Sims, J.; Gray, H. B.; Gross, Z.; Farkas, D. L.; Medina-Kauwe, L. K., A Mechanistic Study of Tumor-Targeted Corrole Toxicity. *Mol. Pharm.* **2011**, *8* (6), 2233-2243.
47. Lim, P.; Mahammed, A.; Okun, Z.; Saltsman, I.; Gross, Z.; Gray, H. B.; Termini, J., Differential Cytostatic and Cytotoxic Action of Metallocorroles against Human Cancer Cells: Potential Platforms for Anticancer Drug Development. *Chem. Res. Toxicol.* **2012**, *25*, 400-409.
48. Sims, J. D.; Hwang, J. Y.; Wagner, S.; Alonso-Valenteen, F.; Hanson, C.; Taguian, J. M.; Polo, R.; Harutyunyan, I.; Karapetyan, G.; Sorasaene, K.; Ibrahim, A.; Marban, E.; Moats, R.; Gray, H. B.; Gross, Z.; Medina-Kauwe, L. K., A Corrole Nanobiologic Elicits Tissue-Activated MRI Contrast Enhancement and Tumor-Targeted Toxicity. *J. Control. Release* **2015**, *217*, 92-101.

49. Haber, A.; Gross, Z., Catalytic Antioxidant Therapy by Metallodrugs: Lessons from Metalloporphyrins. *Chem. Commun.* **2015**, *51* (27), 5812-5827.
50. Okun, Z.; Gross, Z., Fine Tuning the Reactivity of Porphyrin-Based Catalytic Antioxidants. *J. Inorg. Chem.* **2012**, *51* (15), 8083-8090.
51. Okun, Z.; Kupersmidt, L.; Amit, T.; Mandel, S.; Bar-Am, O.; Youdim, M. B. H.; Gross, Z., Manganese Porphyrins Prevent Intracellular Nitration and Subsequent Death of Insulin-Producing Cells. *ACS Chem. Biol.* **2009**, *4*, 910-914.
52. Gross, Z.; Golubkov, G.; Simkhovich, L., Epoxidation catalysis by a manganese porphyrin and isolation of an oxomanganese(V) porphyrin. *Angew. Chem. Int. Ed. Engl.* **2000**, *39* (22), 4045-4047.
53. Kumar, A.; Goldberg, I.; Botoshansky, M.; Buchman, Y.; Z., G., Oxygen Atom Transfer Reactions from Isolated (Oxo)manganese(V) Porphyrins to Sulfides. *J. Am. Chem. Soc.* **2010**, *132*, 15233-15245.
54. Caron, S.; Dugger, R. W.; Ruggeri, S. G.; Ragan, J. A.; Ripin, D. H. B., Large-Scale Oxidations in the Pharmaceutical Industry. *Chem. Rev.* **2006**, *106*, 2943-2989.
55. Baeckvall, J. E., *Modern oxidation methods*. Wiley-VCH Verlag: Weinheim, 2004.
56. Wojaczynska, E.; Wojaczynski, J., Enantioselective Synthesis of Sulfoxides: 2000-2009. *Chem. Rev.* **2010**, *110*, 4303-4356.
57. Hosseini, F.; Golchubian, H., Mn(III)-Catalyzed Oxidation of Sulfides to Sulfoxides with Hydrogen Peroxide. *Tetrahedron Lett.* **2006**, *47* (29), 5195-5197.

58. Kaczorowska, K.; Kolarska, Z.; Mitka, K.; Kowalski, P., Oxidation of Sulfides to Sulfoxides. Part 2: Oxidation by Hydrogen Peroxide. *Tetrahedron* **2005**, *61* (35), 8315-8327.
59. Surendra, K.; Krishnaveni, N. S.; Kumar, V. P.; Sridhar, R.; Rao, K. R., Selective and Efficient Oxidation of Sulfides to Sulfoxides with *N*-Bromosuccinimide in the Presence of Cyclodextrin in Water. *Tetrahedron Lett.* **2005**, *46* (27), 4581-4583.
60. Gross, Z.; Gray, H. B., Oxidations catalyzed by metalloporphyrins. *Adv. Syn. Catal.* **2004**, *346* (2+3), 165-170.
61. Gross, Z.; Galili, N.; Saltsman, I., The First Direct Synthesis of Porphyrins from Pyrrole. *Angew. Chem. Int. Ed.* **1999**, *38*, 1427-1429.
62. Koszarna, B.; Gryko, D. T., Efficient synthesis of meso-substituted porphyrins in a H<sub>2</sub>O-MeOH mixture. *J. Org. Chem.* **2006**, *71*, 3707-3717.
63. Lindsey, J.; Wagner, R. D., Investigation of the synthesis of ortho-substituted tetraphenylporphyrins. *J. Org. Chem.* **1989**, *54*, 828-836.
64. Bard, A. J.; Faulkner, L. R., *Electrochemical Methods: Fundamentals and Applications*. 2nd Ed. ed.; Wiley: New York, 2001.
65. Zhang, R.; Harischandra, D. N.; Newcomb, M., Laser flash photolysis generation and kinetic studies of porphyrin-manganese(V)-oxo intermediates. *Chem. Eur. J.* **2005**, *11* (19), 5713-5720.
66. Chen, T.-H.; Kwong, K.-W.; Carver, A.; Luo, W. L.; Zhang, R., Enhanced iron(III) porphyrin-catalyzed oxidations with iodobenzene diacetate: Synthetic and mechanistic investigations. *Appl. Catal. A* **2015**, *497*, 121-126.

## CURRICULUM VITAE

### Honors and Awards

American Institute of Chemists Outstanding Graduate Student Award	Spring 2017
WKU Analytical Chemistry Award	Spring 2016
Faculty–Undergraduate Student Engagement (FUSE) Grant	Fall 2015
C.P. McNally Undergraduate Scholarship Award	Fall 2015

### Presentations

- **Jeddi, H.;** Zhang, R. (oral presentation, 1<sup>st</sup> place). “Kinetic and Catalytic Studies of Oxidations by an Electron-Deficient Manganese(V)-oxo Corrole.” 102<sup>nd</sup> Annual Meeting of the Kentucky Academy of Science, 2016, Louisville, KY.
- **Jeddi, H.;** Zhang, R. (poster). “Kinetic and Mechanistic Studies of a Manganese(V)-oxo Corrole.” University of Kentucky Undergraduate Research in Chemistry Regional Poster Competition, 2016, Lexington, KY.
- **Jeddi, H.;** Zhang, R. (oral presentation). “Kinetic Studies of Oxygen Atom Transfer Reactions by an Oxo-manganese(v) Corrole.” 46<sup>th</sup> Annual WKU Student Research Conference, 2016, Bowling Green, KY.
- **Jeddi, H.;** Luo, W.; Zhang, R. (poster). “Kinetic and Competition studies of Oxygen Atom Transfer Reactions with a Corrole-manganese(V)-oxo Species.” 251<sup>st</sup> Annual National Meeting of the American Chemical Society, Spring 2016, San Diego, CA.
- **Jeddi, H.;** Luo, W.; Zhang, R. (poster, 1<sup>st</sup> place). “Kinetic and Catalytic Studies of a Corrole-manganese Species.” 101<sup>st</sup> Annual Meeting of the Kentucky Academy of Science, 2015, Highland Heights, KY.
- **Jeddi, H.;** Luo, W.; Zhang, R. (poster). “Synthesis and Kinetic Studies of a Manganese(V)-oxo Corrole.” 67<sup>th</sup> Annual Southeastern Regional Meeting of the American Chemical Society, 2015, Memphis, TN.

### Publications

- Lee, N.F.; Malone, J.; **Jeddi, H.;** Kwong, K.W.; Zhang, R. Visible-Light Photolysis of Corrole-Manganese(IV) Nitrates to Generate Corrole-Manganese(V)-Oxo Complexes. *Inorg. Chem. Commun.* In press.
- Kwong, K. W.; Chen, T.-H.; Luo, W.; **Jeddi, H.;** Zhang, R. A Biomimetic Oxidation Catalyzed by Manganese(III) Porphyrins and Iodobenzene Diacetate. *Inorg. Chim. Acta.* **2015**, *430*, 176–183.

## LIST OF ABBREVIATIONS

---

Ar	Aryl
Al <sub>2</sub> O <sub>3</sub>	Alumina
BF <sub>3</sub> ·OEt <sub>2</sub>	Boron trifluoride diethyl etherate
CYP450s	Cytochrome P450s
DMF	<i>N,N</i> -Dimethylformamide
DDQ	2,3-Dichloro-5,6-dicyanobenzoquinone
FID	Flame ionization detector
GC	Gas chromatography
H <sub>2</sub> TMP	<i>meso</i> -Tetramesitylporphyrin
H <sub>3</sub> TPC	Triphenylcorrole
H <sub>3</sub> TPFC	Tris(pentafluorophenyl)corrole
H <sub>2</sub> O <sub>2</sub>	Hydrogen peroxide
<i>k</i> <sub>obs</sub>	Observed pseudo-first-order rate constant
<i>k</i> <sub>2</sub>	Second order rate constant
LFP	Laser flash photolysis
Mn <sup>III</sup> (TMP)Cl	Tetramesitylporphyrinato manganese(III) chloride
Mn <sup>III</sup> (TPC)	Triphenylcorrolato manganese(III)
Mn <sup>III</sup> (TPFC)	Tris(pentafluorophenyl)corrolato manganese(III)
MS	Mass spectrometry
<i>m</i> -CPBA	<i>meta</i> -Chloroperoxybenzoic acid
NADH	Nicotinamide adenine dinucleotide
NMR	Nuclear magnetic resonance

---

---

PhIO	Iodosylbenzene
PhI(OAc) <sub>2</sub>	Iodobenzene diacetate
ppm	Parts per million
Sub	Substrate
TBHP	<i>tert</i> -Butylhydroperoxide
TON	Turnover number
TMS	Tetramethylsilane
UV-vis	UV-visible

---